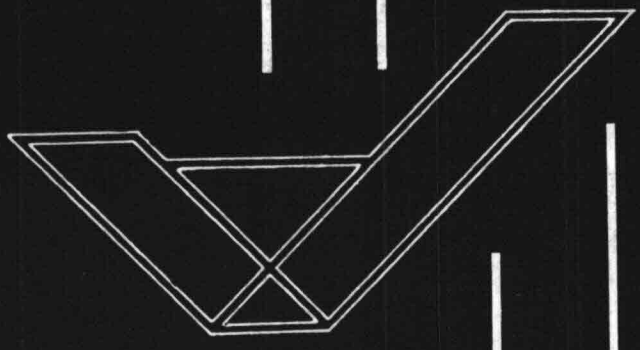

Simulation of main flow and secondary flow in a curved open channel

R. Booij and Joh.G.S. Pennekamp

Report no. 10-83

Laboratory of Fluid Mechanics
Department of Civil Engineering
Delft University of Technology

SIMULATION OF MAIN FLOW AND SECONDARY FLOW IN A CURVED OPEN CHANNEL

R. Booij and Joh.G.S. Pennekamp

Report No. 10 - 83

Laboratory of Fluid Mechanics

Department of Civil Engineering

Delft University of Technology

Summary

Knowledge of the secondary flow is essential for predictions about the morphology of alluvial bottoms in tidal channels. In this research the determination of the secondary flow is based on a known depth averaged velocity field. The depth averaged velocities must be computed with a high accuracy in order to make possible a reasonable determination of the secondary flow. The depth averaged velocities are computed from the shallow water equations. These equations are solved by means of an implicit finite difference method of the ADI-type. The reproduction of the depth averaged flow with the generally used partly explicit ADI-method appeared not to be usable for the flow in tidal channels, because of a large diffusion coefficient, required to obtain stability.

In this report a fully implicit ADI-method is considered. The simulation of the steady flow in a curved flume with the geometrical proportions of a river is compared to measurements. The reproduction of the depth averaged velocity field is satisfactory. A disturbance connected with the irregular numerical representation of the sidewalls will be much smaller in a tidal channel.

The secondary flow, assumed fully developed, is computed, based on this depth averaged velocity, and compared to the measurements. The agreement is reasonable, especially when the narrowness of the flume and the connected severe influence of the disturbances at the sidewalls on the radius of curvature of the flow is considered.

Contents

List of figures

1. Introduction

Predictions about the morphology of alluvial bottoms in rivers and tidal channels require a thorough knowledge of the flow pattern. In particular the description of the secondary flow is important,because it gives rise to bottom slopes transverse to the main flow. In tidal channels two contributions to the secondary flow have to be considered, secondary flow caused by the curvature of the main flow, especially in bends of the tidal channels, and secondary flow caused by the Coriolis acceleration induced by the rotation of the earth (Booij and Kalkwijk,1982). Both these contributions to the secondary flow may in many cases be assumed to be fully developed. The validity of this assumption depends on the variation of the bottom topography and of the velocity and curvature of the main flow. Considerable variations in the longitudinal direction over less than about 30 h, where h is the depth of the flow, or over a time less than about 30 h/u_s, where $\bar{u}_s$ is the depth averaged main flow velocity, can have an important influence on the development of the secondary flow (Booij and Kalkwijk, 1982).

This research is financially supported by the directorate of the Deltadienst of Rijkswaterstaat. It concerns the determination of the secondary flow in tidal channels of estuaries like the Eastern Scheldt, to make possible predictions about the morphology, with a view to the changes in bottom topography expected to be induced by the partial enclosure of this estuary. The computation of the secondary flow is based upon a known depth averaged velocity field. The depth averaged velocities must be computed with a high accuracy in order to make possible a reasonable determination of the secondary flow. For the computation of the depth averaged velocities usually an implicit finite difference method of the ADI-type is used. In these methods the depth averaged equations of motion and the depth averaged continuity equation, together called the shallow water equations, are solved by means of an Alternating Direction Implicit computation using a spatial staggered grid. A simplification of the effective stress term in the shallow water equations is made to economize the computation.

Although the velocity and waterlevel parameters are treated implicitly, in general the convective and diffusion terms however are represented explicitly in the difference equations. This explicit representation can give rise to instability of the numerical computation.

The computation has to be executed with an imposed diffusion coefficient in order to suppress this instability (Vreugdenhil and Wijbenga, 1982). In the simulation of the flow in rivers and tidal channels, and in Laboraty flumes, this imposed diffusion coefficient appears, however, to be much larger than the physical lateral eddy viscosity. Such a large diffusion coefficient severely hampers the representation of the velocity distributions (Pennekamp and Booij, 1983, and Booij, 1983). Recently the Dienst Informatieverwerking of Rijkswaterstaat developed a fully implicit finite difference method of the ADI-type. This method is usually referred to as Miniwaqua. An important characteristic of this method is the separate treatment of the convective terms in such a way that problems concerning the boundary values are avoided (Stelling, 1983). In this report the reproduction of the main flow field using this fully implicit method is investigated. The computations are executed for steady flow in a curved flume of the Delft Hydraulics Laboratory with two different bottom topographies: a plane bed (de Vriend and Koch, 1977) and an uneven bed (de Vriend and Koch, 1978). Both flow configurations allow extensive comparisons with measurements and other numerical models.

Based upon the calculated main flow, the secondary flow is derived and is compared to the measured secondary flow.

2. Mathematical description

2.1. The shallow-water equations

Open channel flows with very small vertical accelerations have a hydrostatic pressure distribution along each vertical. Most flow problems in rivers and estuaries belong to this category. Integration over the depth of the Reynolds' equations for turbulent flow yields, using this assumption, the differential equations for two-dimensional horizontal flow, the shallow water equations (Flokstra, 1976), which read:

$$\frac{\partial u}{\partial t} + u\frac{\partial u}{\partial x} + v\frac{\partial u}{\partial y} + g\frac{\partial \zeta}{\partial x} + \frac{1}{\rho h}(\tau_{bx} - \tau_{wx}) - \Omega v + $$

$$- \frac{1}{\rho h}\frac{\partial (hT_{xx})}{\partial x} - \frac{1}{\rho h}\frac{\partial (hT_{xy})}{\partial y} = 0 \qquad (1)$$

$$\frac{\partial v}{\partial t} + u\frac{\partial v}{\partial x} + v\frac{\partial v}{\partial y} + g\frac{\partial \zeta}{\partial y} + \frac{1}{\rho h}(\tau_{by} - \tau_{wy}) + \Omega u + $$

$$- \frac{1}{\rho h}\frac{\partial (hT_{xy})}{\partial x} - \frac{1}{\rho h}\frac{\partial (hT_{yy})}{\partial y} = 0 \qquad (2)$$

$$\frac{\partial \zeta}{\partial t} + \frac{\partial (hu)}{\partial x} + \frac{\partial (hv)}{\partial y} = 0 \qquad (3)$$

In these equations the following notation is used (see also definition sketch, fig. 1):

x,y	horizontal coordinates, z is the vertical coordinate;
t	time;
u,v	depth-averaged velocity-component in x-,y-direction;
ζ	waterlevel above reference level;
g	acceleration due to gravity;
h	waterdepth;
ρ	mass density;
τ_{bx}, τ_{by}	components of bottom shear stress;
τ_{wx}, τ_{wy}	components of surface shear stress;
Ω	Coriolis parameter: $2\omega \sin\phi$,where ϕ is the geographic latitude and ω is the angular velocity of the rotation of the earth;
T_{xx}, T_{xy}, T_{yy}	effective stresses in vertical planes.

Usually the bottom shear stresses are assumed to act opposite to the direction of the mean velocity vector and to vary with the mean velocity squared:

$$\tau_{bx} = \frac{\rho g}{C^2} u \sqrt{u^2+v^2} \tag{4}$$

$$\tau_{by} = \frac{\rho g}{C^2} v \sqrt{u^2+v^2} \tag{5}$$

where C is the Chézy coefficient.

In current numerical models the effective stresses are replaced by diffusion terms, with an isotropic diffusion coefficient , ε_p , which is constant in time and throughout the flow (Vreugdenhil and Wijbenga, 1982; Booij and de Boer, 1981). With the bottom stress assumption (eqs. 4 and 5) and the constant diffusion coefficient, the shallow water equations (eqs. 1,2 and 3) can be rewritten into:

$$\frac{\partial u}{\partial t} + u\frac{\partial u}{\partial x} + v\frac{\partial u}{\partial y} + g\frac{\partial \zeta}{\partial x} + \frac{g}{C^2}\frac{u\sqrt{u^2+v^2}}{h} - \frac{\tau_{wx}}{\rho h} - \Omega v$$

$$- \frac{\partial}{\partial x}(\varepsilon_p \frac{\partial u}{\partial x}) - \frac{\partial}{\partial y}(\varepsilon_p \frac{\partial u}{\partial y}) = 0 \tag{6}$$

$$\frac{\partial v}{\partial t} + u\frac{\partial v}{\partial x} + v\frac{\partial v}{\partial y} + g\frac{\partial \zeta}{\partial y} + \frac{g}{C^2}\frac{v\sqrt{u^2+v^2}}{h} - \frac{\tau_{wy}}{\rho h} + \Omega u$$

$$- \frac{\partial}{\partial x}(\varepsilon_p \frac{\partial v}{\partial x}) + \frac{\partial}{\partial y}(\varepsilon_p \frac{\partial v}{\partial y}) = 0 \tag{7}$$

$$\frac{\partial \zeta}{\partial t} + \frac{\partial (hu)}{\partial x} + \frac{\partial (hv)}{\partial y} = 0 \tag{8}$$

These shallow water equations can be solved numerically. Most numerical models used for the integration of these shallow water equations are based on the implicit finite difference ADI-scheme proposed by Leendertse, (1967).

The effective stresses T_{xx}, T_{xy}, and T_{yy} are combinations of viscous stresses, Reynolds' stresses, and momentum fluxes due to the non-uniform distributions of the velocities over the depth. For the flow configurations considered in this investigation the viscous stresses can be neglected in comparison with the Reynolds' stresses. The momentum fluxes due to the non-uniform distributions of the velocities are negligible when the secondary flow is not important. When on the other hand secondary flow is important, then these momentum fluxes can not be neglected, but they can certainly not be represented by diffusion terms (Pennekamp and Booij, 1983).

When the effective stresses are replaced by diffusion terms, the best choice for the diffusion coefficient is the lateral eddy viscosity coefficient, ν_t. Then the lateral depth-averaged Reynolds'stresses, which are the most important, are best accounted for. For wide straight channels Fischer et al. (1979) mention

$$\nu_t = 0.15\, u_* h \tag{9}$$

with u_* the friction velocity

$$u_* = \frac{\sqrt{g}}{C} (u^2+v^2)^{\frac{1}{2}} \tag{10}$$

The value of the Chézy coefficient C varies generally from 40 to 60 $m^{\frac{1}{2}}/s$. Expression (9) gives at these values

$$\nu_t = 0.01\, h\, (\, u^2 + v^2\,)^{\frac{1}{2}} = 0.01\, h u_s \tag{11}$$

This expression of the lateral eddy viscosity can be used for most channels and rivers with gentle bends and smooth sides.

2.2. Secondary flow

The flow pattern in river and channel bends is quite complex. In addition to the main flow, defined by the horizontal velocity component, u_s, in the direction,s, of the depth averaged velocity, a secondary flow, defined by the horizontal velocity component, u_n, in the normal direction, n, can be important. The main flow velocity can be described properly by its depth averaged value, $\bar{u}_s$,but the depth averaged value of the secondary flow velocity is zero. The secondary flow can be described by its intensity, i.e. half the averaged absolute value (de Vriend, 1981),

$$I_n = \frac{1}{2h} \int_{depth} |u_n| \, dz \tag{12}$$

The secondary flow is a combination of two contributions, the secondary flow caused by the curvature of the main flow, u_n^b, and the secondary flow caused by the Coriolis acceleration, u_n^c, (Booij and Kalkwijk, 1982)

$$u_n = u_n^b + u_n^c \tag{13}$$

u_n^b and u_n^c are given by (de Vriend, 1976 ; Booij and Kalkwijk, 1982)

$$u_n^b = \alpha \frac{\bar{u}_s}{\kappa^2} \frac{h}{R} f_b\left(\frac{z}{h}, \frac{C}{\sqrt{g}}\right) \tag{14}$$

and

$$u_n^c = \alpha' \frac{\Omega h}{\kappa^2} f_c\left(\frac{z}{h}, \frac{C}{\sqrt{g}}\right) \tag{15}$$

In these equations f_b and f_c are complicated functions of the vertical coordinate and of the Chézy coefficient; κ is von Karman's constant; R is the radius of curvature of the main flow; and α and α' are parameters that indicate the degree of development of the secondary flow components.

The secondary flow contribution caused by the Coriolis acceleration is important in tidal channels but is negligible in flume experiments and in most rivers, because of the small value of Ωh. The secondary flow intensity is then given by

$$I_n = \alpha \, c_b \left| \frac{\bar{u}_s}{\kappa^2} \frac{h}{R} \right| \tag{16}$$

where c_b is half the depth averaged absolute value of f_b

$$c_b = \frac{1}{2h} \int_{depth} \left| f_b\left(\frac{z}{h}, \frac{C}{\sqrt{g}}\right) \right| dz \tag{17}$$

c_b is a function of the Chézy coefficient only. The value of c_b as a function of C is given in fig. 2.

The overbar in the depth averaged velocities is henceforth dropped. Further a fully developed secondary flow is assumed, so expression (16) for the secondary flow intensity becomes

$$I_n = c_b \left| \frac{u_s}{\kappa^2} \frac{h}{R} \right| \tag{18}$$

To compute the secondary flow intensity in a point from the main flow distribution, the radius of curvature of the main flow, R , in that point has to be known. A simple expression for R can be derived in a cartesian coordinate system with one of the axes in the direction, s , of the depth averaged velocity, u_s, and the other axis, n, in the horizontal direction perpendicular to s (see fig. 3)

$$\frac{1}{R} = \frac{1}{u_s} \frac{\partial u_n}{\partial s} \tag{19}$$

The depth averaged velocity in the n-direction, u_n , is zero in the point considered, but its derivative in a curved flow is not. Transformation to the x,y-coordinate system, using

$$\begin{pmatrix} s \\ n \end{pmatrix} = \begin{bmatrix} \cos\theta & \sin\theta \\ -\sin\theta & \cos\theta \end{bmatrix} \begin{pmatrix} x \\ y \end{pmatrix} \tag{20}$$

where θ is the local angle between mean flow direction and x-direction, yields (see eq. 19)

$$\frac{1}{R} = \frac{1}{u_s} \left(\frac{\partial u_n}{\partial x} \frac{\partial x}{\partial s} + \frac{\partial u_n}{\partial y} \frac{\partial y}{\partial s} \right) = \frac{1}{u_s} \left(\cos\theta \frac{\partial u_n}{\partial x} + \sin\theta \frac{\partial u_n}{\partial y} \right) \tag{21}$$

This can be elaborated into

$$\frac{1}{R} = \left(\sin\theta \cos\theta \frac{\partial u}{\partial x} + \cos^2\theta \frac{\partial v}{\partial x} - \sin^2\theta \frac{\partial u}{\partial y} - \sin\theta \cos\theta \frac{\partial v}{\partial y} \right) \cdot \frac{1}{(u \cos\theta - v \sin\theta)} \tag{22}$$

This expression can be used for the computation of R from the output of ADI-type simulations when the partial differential equation is approximated by a finite difference equation. The expression contains relations between velocities and spatial parameters in both directions, therefore the obvious difference molecule, on which the difference equation is based, has a cross-like shape (see fig. 3).

The accuracy of the finite difference equation is dependant on the amount of grid points that the difference molecule covers. A difference molecule with a fourth order truncation error contains at least five successive grid points; e.g.

$$\left.\frac{\partial u}{\partial x}\right|_i = \frac{u_{(i-2)} - 8u_{(i-1)} + 8u_{(i+1)} - u_{(i+2)}}{12\Delta} + O(\Delta^4) \qquad (23)$$

whereas a less accurate difference molecule covering only three successive points introduces a second order truncation error; e.g.

$$\left.\frac{\partial u}{\partial x}\right|_i = \frac{-u_{(i-1)} + u_{(i+1)}}{2\Delta} + O(\Delta^2) \qquad (24)$$

The subscripts in eqs. 23 and 24 indicate the different grid points considered.

Using equation (23) in the differential equation (22) means that the radius of curvature cannot be computed nearer to the boundaries than two grid spacings, which proved very awkward in the processing of the simulated depth averaged flow, considered in this report, because of the narrowness of the flume. With a decline in accuracy, equation (24) can be used near the boundaries.

3. The flow Configurations

An important aspect of this investigation is the accuracy of the reproduction of the depth averaged velocity field in a tidal channel. From this depth averaged velocity field the secondary flow , which has a considerable influence on the morphological behaviour, is computed. The reproduction of the depth averaged velocity field can only be considered when the flow configuration to be reproduced is known with enough precision and detail.This restricts a possible verification of flows to flows in Laboratory flumes mainly.

3.1. Channel geometry

The calculations are executed for a flume in the Delft Hydraulics Laboratory, called the DHL-flume in this report. In this large flume, with a rather gentle bend (B/R_f = 0.12, with B the width and R_f the radius of curvature of the channel axis) of almost 90^o, extensive measurements were executed for two different bed configurations. In the first series of experiments the bed of the flume was plane and the cross-section rectangular (see fig. 4) (deVriend and Koch, 1977). In the other series of experiments the flume was provided with a fixed uneven bottom of more or less the same shape as in a natural river bend (see fig. 5)(de Vriend and Koch, 1978). The flume with the uneven bed is then also a fair model of a bend in a tidal channel (Pennekamp and Booij, 1983). In addition to the measurements various mathematical models, two- and three-dimensional, were used to reproduce the flow (Kalkwijk and de Vriend, 1980; de Vriend, 1981). The measurements and the computations were limited to steady flow. The cross-sections in which the measurements were executed are indicated in fig. 4 and fig. 5.

The flow is mainly controlled by the bottom friction. The distributions of the depth averaged velocity in the cross-sections reflect therefore mainly the depth distributions. Deviations from the measurements are somewhat easier to analyse in the plane bed configuration then they are in the uneven bed configuration . Besides the sidewall boundary effects are much larger in the plane bed configuration, especially when using a square computational grid (see Ch. 3.2.).

The plane bed configuration is properly speaking too strong a test for the reproduction of flow in a tidal channel. It gives, however, an indication of the results that can be expected from the reproduction of the measurements in a varying flow planned for the bend flume with rectangular cross-section in the Laboratory of Fluid Mechanics of the Delft Technical University within the framework of this investigation.

3.2. Computational grid

For the computations of the depth averaged velocity field with Miniwaqua a square grid with a distance between neighbouring grid points $\Delta = 0.40$ m was used (see fig. 6a). At this grid spacing the number of grid points used in the computation is about 3700. For the time being Miniwaqua requires however memory space for the circa 22,000 grid points covering the rectangle that encloses the complete flume. This was close to the maximum of 27,000 grid points allowed by the used computer, so $\Delta = 0.40$ m is close to the smallest grid spacing possible. To examine the influence of the grid spacing also some computations with $\Delta = 0.60$ m were executed.

The time step used was $\Delta t = 1.5$ s. Time steps of 3 s and of 0.75 s were used in some computations to examine the influence of the time step on the result of the computations. The computations with $\Delta t = 3$ s showed the beginning of a declining accuracy at larger time steps, especially in the plane bed configuration. At this time step wavelike disturbances following the grid lines arise.

Curved sidewalls of flumes and rivers bring about irregular boundaries when a square or rectangular grid is used in the numerical computations. Irregular boundaries can give rise to errors in the computations (Kuipers and Vreugdenhil, 1973; Weare, 1979). A more natural choice of the grid configuration of the sidewalls and the bed is not yet possible in Miniwaqua, although it is planned to modify Miniwaqua in this respect. Other methods of integrating the shallow water equations that allow non-rectangular grid configurations are not yet usable for the computation of a time varying flow like the flow in a tidal channel with sufficient accuracy and a reasonable time step.

In fig. 7 the grid configuration is given as it is used by de Vriend (1981) for computations with various two- and three-dimensional models of the flow in the DHL-flume with plane bed.

4. Lateral viscosity

In implicit finite difference methods of the ADI-type with the explicit representation of convective and diffusive terms, a lateral diffusion coefficient, ε , has to be imposed in order to suppress instabilities caused by truncation errors. The required diffusion coefficient depends on the time step, Δt ,and the grid spacing, Δ , used. Two stability criteria can be derived (Pennekamp and Booij, 1983)

$$\varepsilon > \beta \, u_s^2 \, \Delta t \qquad (25)$$

,where the value of the coefficient β depends on the exact computational model used, and

$$\varepsilon < \frac{\Delta^2}{2\Delta t} \qquad (26)$$

In computations of the authors with a computational model of this kind, TIDES , β had a value of about 0.12. The computations concerned the flow in the straight part of the DHL-flume. The depth averaged velocities were around 0.40 m/s . Criteria (25) and (26) yield then a maximum time step of about 2s for Δ = 0.40 m. This maximum time step requires, however, a lateral diffusion coefficient $\varepsilon \simeq 0.04$ m^2/s . (See fig. 8). This value is to be compared to the assumed eddy viscosity coefficient $\nu_t \simeq 0.001$ m^2/s (see eq. (11)) for h = 0.25 m). The use of a diffusion coefficient that is much larger than the eddy viscosity, has severe consequences for the velocity field computed in rivers, tidal channels and resembling flumes (Pennekamp and Booij, 1983; Booij, 1983), and therefore for the calculations of the secondary flow and the connected sediment transport. The stability criteria allow a realistic diffusion coefficient, but only in combination with a prohibitively small time step. ($\Delta t \lesssim 0.05$ s for $\varepsilon = 0.001$ m^2/s , see fig. 8).

A fully implicit computational model is unconditionally stable and so no diffusion coefficient is required for stability. Truncation errors can, however, give rise to a numerical viscosity. In Miniwaqua this numerical viscosity seems to be unimportant. Computations with Miniwaqua of the depth averaged velocity field in the straight part of the DHL-flume showed no apparent additional viscosity (see fig. 9).

The distribution across the flume of the depth averaged velocity was almost completely determined by the bottom topography as expected (Pennekamp and Booij, 1983). The situation in the bent part of the flume is less clear (see chapter 5). The irregular boundaries in a bend, when using a square grid, can give rise to an additional influence of the boundary (Weare, 1979). The combination diffusion coefficient - time step in Miniwaqua means an important improvement over the partly explicit ADI-method, at least in the straight section of the flow (see fig. 8).

All computations were executed with a free-slip boundary condition

$$\left.\frac{\partial u_s}{\partial n}\right|_{wall} = 0 \qquad (27)$$

The direction of n is perpendicular to the wall. The no-slip boundary condition

$$u_s \Big|_{wall} = 0 \qquad (28)$$

, though physically more attractive, causes an influence of the sidewalls that is too extensive, especially in case of a large grid spacing. A large grid spacing is inevitable in gentle bends like the bends in rivers, tidal channels and flumes like the DHL-flume. The mathematical no-slip condition is not equivalent with the physical no-slip condition in this case, because the lateral eddy viscosity decreases rapidly near the sidewalls, whereas the diffusion coefficient in the mathematical model is maintained at a constant value. The ill-matching of the grid boundaries and the real boundaries in the bend can worsen this effect.

5. Reproduction of the velocity field

The first reproduction of a depth averaged velocity field tried with Miniwaqua concerned a flow in the DHL-flume with uneven fixed bed, as this configuration came closest to the flow in a tidal channel, aimed at in this investigation. To explain some deviations of this reproduction from the measurements and from other 2-dimensional models by de Vriend, 1981, reproduction of the flow in the DHL-flume with a plane bed was executed. This latter configuration is dealt with first.

5.1. Reproduction in the plane bed configuration

In fig. 10 the depth averaged velocity field of the DHL-flume with plane bed configuration as computed with Miniwaqua is plotted. The grid distace, Δ , is 0.40 m and the time step Δt = 1.5 s . In fig. 11 the surface level is plotted. To compare the results with the measured velocity field and with the results of other computational models, the depth averaged velocity at some cross-sections are plotted separately in fig. 12. The velocities at all the grid points within a strip with a width of 1.5 m around each cross-section are used to compose the plot, in order to provide a better velocity distribution by the inclusion of more grid points. The use of this relatively broad strip also gives an estimate of the scatter in the velocity distribution.

The reproduction of the velocity distribution over the cross-sections is on the whole not bad, but certain defects remain. To analyse the defects of the reproduction a discussion of the expected velocity field is given first.

In the straight part of the flume the velocity distribution will be flat but for the small boundary layers at the sidewalls with widths of about 2h. In these boundary layers the no-slip condition and the lateral eddy viscosity slow down the flow. This boundary layer will not be reproduced in the computation because of the used free-slip boundary condition.

The bend can be divided in two parts. In the first part of the bend (and in the last section of the straight part of the flume) the flow adapts to the conditions prevailing in the bend, where a surface gradient in the lateral direction forces the flow through the bend. In the second part the flow is more or less adapted to the bend. Then a balance between the longitudinal surface gradient and the bed shear stress applies, when secondary flow and lateral diffusion can be left out of consideration. Equations (6) and (7) simplify in the flow direction to

$$g \frac{\partial \zeta}{\partial s} + \frac{g}{C^2} u_s^2 = 0 \qquad (29)$$

or

$$u_s = C \left(- \frac{\partial \zeta}{\partial s}\right)^{\frac{1}{2}} \qquad (30)$$

The surface gradients in the cross-sections are equal in this equilibrium region, so the longitudinal surface gradient is inversely proportional to the distance to the center of curvature of the flume , r ,

$$\frac{\partial \zeta}{\partial s} = \frac{\Delta h/\Delta s}{r/R_f} \qquad (31)$$

, with $\Delta h/\Delta s$ the surface gradient along the channel axis. Equation (31) substituted in equation (29) yields (see fig. 13)

$$u_s = \left(\frac{R_f}{r} \right)^{\frac{1}{2}} \frac{(-\Delta h/\Delta s)^{\frac{1}{2}}}{C} \qquad (32)$$

The depth averaged velocity is inversely proportional to the root of the distance to the center of curvature of the flume. Equations (6) and (7) give in radical direction

$$g \frac{\partial \zeta}{\partial n} - \frac{u_s^2}{r} = 0 \qquad (33)$$

For the DHL-flume with $u_s \approx 0.4$ m/s this gives a difference in surface level between outer and inner side of the bend of about 2mm (see fig. 14).

In the first part of the bend and the last section of the straight part of the DHL-flume the flow has to adapt to the equilibrium distribution of the bend. In this part of the flume the flow resembles a potential flow. The reason for this resemblance to a potential flow is the negligibility of the differences of the bed shear stress over

the cross-sections. Consequently the velocity distributions over the cross-sections are mainly determined by the differences between the longitudinal surface gradients over the cross-sections in this part of the flow. The flow however is not a potential flow as the bed shear stress itself cannot be neglected. The difference between the initial horizontal surface level and the difference of 2 mm between the outer and the inner side of the equilibrium flow in the bend, bring about a larger drop of the surface on the inner side of the bend and correspondingly a larger velocity. The velocity difference corresponding with a difference of 2 mm in radial surface level is about 0.05 m/s.

Secondary flow transports the higher velocities to the outer side and the smaller velocities to the inner side of the bend. As the secondary flow velocities are quite small because of the small depth and the large radius of curvature, this effect is not important in the first part of the bend. After about 20^{o} these transport effects of the secondary flow can become appreciable.

The velocity field computed with Miniwaqua for the plane DHL-flume shows roughly the behaviour described above. Only the ill-matching of the square grid configuration with the direction of the flume in the bend appears to have severe effects on the reproduction of the flow. Two deviations caused by this grid configuration effect can be distinguished (see Ch 5.2). The first deviation is a large scatter of the velocities near the outer wall in the first half of the bend and near the inner wall in the second half of the bend. The second deviation is a slowing down of the flow near the inner wall in the first half of the bend and near the outer wall in the second half. This can not be caused by a wall shear stress as a free-slip boundary condition was used. The flow appears not to be able to follow the bend. The region in which the flow is slowed down grows in the flow direction in both parts of the bend.

In the straight part of the flume, the cross-sections at - 23.0 m - 11.5 m and 0^{o} show almost flat velocity profiles in accordance with the measurements, which show the same profiles except for an inflow disturbance near the centre and a small boundary layer effect.

The transition of the flow in the straight part of the flume to a flow that is adjusted to the curvature of the bend shows the resemblance to potential flow as discussed above. In this respect the

computed velocity profiles correspond better to the measurements than the profiles computed with two- and three-dimensional models used by de Vriend (1981). The latter show a somewhat exaggerated acceleration of the flow at the inner side of the bend at 0^{o} and too small a radial velocity gradient in comparison with potential flow at 138^{o}.

The velocity profiles in the last part of the bend, at the cross-sections at 55^{o}, 68.8^{o} and 82.5^{o} resemble the equilibrium profile in the middle of the flume. The profiles are however spoiled by the influence of the grid configuration effects in this part of the bend and by remainders of former grid configuration effects.

The influence of the secondary flow on the distribution of the main flow velocity is not simulated by the two-dimensional computations considered here. Between the cross-sections at 27.5^{o} and 41.3^{o} the effect of the displacement of the main flow to the outer wall by the secondary flow is suggested. This displacement originates probably from the grid configuration effect and partly from the large velocity gradients at the cross-section at 13.8^{o}. The large bed shear stress caused by the high velocities near the inner wall may bring about surface gradients that accelerate the flow near the outer wall.

The time step used was close to an optimum. Doubling the time step brought about wavelike disturbances in the surface level while computations with half the time step resulted only in very small changes. Computations with a grid spacing $\Delta = 0.60$ m only worsened the grid configuration effect (see fig. 15).

5.2 Grid Configuration effects

The direction of the side wall of the flume with respect to the grid configuration has important consequences for the exact form of the numerical boundary and, with that, of the velocity field computed. At the outer side wall of the first part of the bend and the inner side wall of the last part, the flow runs from time to time into an obstruction (see fig. 16). The flow is accelerated at the contraction and decelerates gradually behind the contraction because of the small angle of the boundary behind the contraction with the flow direction. The sudden displacements of the flow will cause a relatively large scatter in the velocity profile.

At the inner side wall in the first part of the bend and at the outer side wall in the last part a totaly different situation occurs. Sudden widenings of the numerical flume arise (see fig. 17).

Eddies would occur if the widenings contained more grid points. The flow only slowly fills up the widened flow field, with the result that the second widening takes place before the velocity in the first is adjusted.

To investigate the influence of the side walls, computations in a straight channel for various orientations of the grid configuration with respect to the channel axis are planned, as well as a computation of the DHL-flume with a 45^{o} degrees rotated grid configuration.

The various grid configuration effects will bring about a larger energy dissipation because of the differences in velocity. The bed shear stress increases as it is quadratic in the velocity. The larger energy dissipation is reflected in a larger surface slope (see fig. 18).

Weare (1979) concluded, on the ground of a computation of a channel lying at 45^{o} with respect to the grid direction, that the inaccuracy connected with the grid configuration effect depended on the Courant number. This appeared not to be true in our computations. Halving the time step hardly influenced the results. Enlarging the grid point distance from $\Delta = 0.40$ m to $\Delta = 0.60$ m increased the grid configuration effect, whereas the Courant number declines, so the accuracy should increase according to Weare. The remark of Weare that the boundary conditions effectively impose a no-slip condition at irregular boundaries can be endorsed but the diffusion of the effect of the no-slip constraint into the rest of the solution by the second order truncation error is not apparant in this numerical scheme.

5.3. Reproduction in the uneven bed configuration

The results of the computation with Miniwaqua of the depth averaged velocity field in the DHL-flume with uneven bed configuration are given in figs. 19 to 22. In fig. 19 the depth averaged velocity field is plotted and in fig. 20 the surface level field. The profiles of the depth averaged velocity at the chosen cross-sections are plotted in fig. 21. The difference of the surface levels of the outer and the inner side of the bend are given in fig. 22.

The computed flow is roughly similar in character to the flow in the plane bed configuration. The reproduction in the straight part of the flume and in the first part of the bend is good.

The shifting of the maximum velocity to the inner side of the bend, the potential flow effect, is correctly reproduced (see fig. 21), as is the difference of the surface levels of the outer and inner side (see fig. 22).In the values of the surface levels in fig. 22 the surroundings of each point had to be accounted for because of the large scatter in the computed surface levels near the sides (see fig. 20).(The scatter in the plane bed configuration (see fig. 11) was even worse, making the differences in surface levels in fig. 14 less accurate.)

The various models considered by de Vriend (1981) in general give comparable velocity distributions in this section of the flume, but they fail in reproducing the correct surface gradient across the flume. An improved version (see Olesen, 1982) of the simplified model by Kalkwijk and de Vriend (1980) yields a reasonable reproduction of the surface gradients connected with the potential flow effect.

In the first half of the bend, the place in the cross-sections where the velocity is at maximum crosses the deepest part of the flume to the outer side of the bend in the uneven bed configuration (see fig. 21). This is probably caused mainly by the same grid configuration effect, as encountered in the plane bed configuration. The slowing down of the flow at the inner side wall is obvious, but less important because of the shallower flow at the sides in the uneven bed configuration. Another cause of the outward movement of the maximum velocity can again be the surface level reaction on the slowing down of the high velocity at the inner side, because of the potential flow effect, after the first part of the bend.

In the second half of the bend the maximum velocity again crosses the main channel, back to the inner side of the deepest part of the flume as a reaction to the grid configuration effect on the outer side (see fig. 21).

The magnitude of the grid configuration effect was again larger when the grid $\Delta = 0.60$ m was used (see fig. 23).

Halving the time step or using a zero lateral eddy viscosity did not change the results appreciably. Another way of treating the side wall boundary and applying different outflow boundary conditions yielded hardly any difference in the flow field. The latter effect corresponds to the small influence of the (physical) outflow boundary in the prototype. A slightly lower bed roughness gave a slightly smaller longitudinal surface gradient, without changing however the shape of the velocity profiles. This all leads to the conclusion that the strong slowing down of the velocity at the side wall in some parts of the flow is indeed an effect that depends mainly on the relation between the direction (and spacing) of the grid and the position of the flume.

The width to depth ratio is more favourable in a tidal channel and the side walls have less influence there, so a better reproduction can be expected in a tidal channel, compared to the DHL-flume. Variations in the bed level are less critical concerning the grid configuration than side walls, as the bottom is smoothed by interpolation in Miniwaqua (see fig. 5b), leading to a much better reproduction of the flow in a tidal channel.

A better reproduction will probably have to await the possibility of using grid configurations that fit better with the bottom configuration and especially with the side walls.

6. The reproduction of secondary flow

Based on the computed depth averaged flow the intensity of the secondary flow is calculated using equation (18). The secondary flow is assumed to be fully developed. This assumption will only cause minor deviations as the variations of the bottom in the longitudinal direction are only very gradual in the DHL-flume (Booij and Kalkwijk, 1982). The values of the variables u_s,h and c_b follow directly from the local values of the depth averaged flow field.

The curvature of the depth averaged flow, R , is calculated with equation (22), using a difference molecule with a cross-like shape (see fig. 3). In the body of the fluid a difference molecule containing five successive grid points, introducing a fourth order truncation error, (see eq. 23) is used. Near the boundaries a difference molecule containing three successive grid points, , connected with a second order truncation error, is used (see eq. 24). In fig. 24 the radius of curvature field is given for the uneven bed configuration. Reliable values of R are expected in the middle part of the flume but not near the side walls. There the large scatter of the depth averaged velocity values caused by the grid configuration is amplified in the determination of R. This effect will be much less serious in a tidal channel because of the smaller influence of the side walls.

The computation of the secondary flow intensity can only yield reliable values when the depth, the depth averaged velocity and the curvature of the depth averaged flow are determined with satisfactory accuracy. The value of R is the most critical. This again excludes the regions near the side wall boundaries.

In fig. 25 the secondary flow intensity in the chosen cross-sections is given for the plane bed configuration and in fig. 26 for the uneven bed configuration. In both cases the secondary flow is too small compared with the values obtained by the measurements of de Vriend and Koch (1977,1978). This corresponds to the values obained from secondary flow computations by de Vriend and Koch, who advise a multiplication of the computed values by about $1\frac{1}{3}$ to obtain the measured secondary flow intensity.

It is not known if the source of this discrepancy is a less appropriate assumption of the viscosity distribution or of the bed shear stress in the derivation of expression (14), or an imperfection of the measurements. Perhaps measurements of the Reynolds' stresses, the secondary flow and the steady main flow executed in a curved flume in the Laboratory of Fluid Mechanics of the Delft Technical University will shed light on this problem.

Except for the side wall regions the computed values of the secondary flow show a reasonable agreement with the measured values when the correction with the factor $1\frac{1}{3}$ is applied. The side wall regions are relatively large because of the narrowness of the flume. In tidal channels the side wall regions, where no reliable values for the secondary flow will be found, are much smaller.

7. Conclusions

The reproduction of the depth averaged velocity field in a large flume of the Delft Hydraulics Laboratory, a model of a river bend, with a fully implicit finite difference method of the ADI-type, Miniwaqua, developed at the DIV of Rijkswaterstaat, is satisfactory. This is an important amelioration with respect to the partly explicit methods of the ADI-type, which require a large diffusion coefficient in order to obtain stability.

In the first part of the bend, where the flow has the character of a potential flow, the computations yield velocities and surface elevations that compare very good with the measurements. In this part of the flume the reproduction of the flow by Miniwaqua is better than by the various models used by de Vriend (1981).

Further down the bend (after about 20^{o}) disturbances at the sidewalls develop. These disturbances are connected with the numerical representation of the sidewalls in the bend. At the side where the grid configuration has the effect of a widening of the flow, a growing disturbance appears. At the side where the grid configuration has the effect of an obstruction of the flow, a large scatter of velocity and surface level values occurs. These grid configuration effects are more important in the plane bed configuration of the flume, where large sidewalls are present, than in the uneven bed configuration. In the reproduction of the flow in a tidal channel, this effect will be less important, due to the larger width to depth ratio and the absence of vertical sidewalls.

The influence of the secondary flow on the main flow cannot be reproduced by Miniwaqua. This influence is not very large because of the gentle curvature of the flume.

The reproduction of the secondary flow is reasonable. The values are a factor $1\frac{1}{3}$ low compared to the measurements. This discrepancy between computed values and measured values of the secondary flow in the DHL-flume was already observed by de Vriend and Koch (1977, 1978) and de Vriend (1981). The cause is not yet known. It may originate from an incorrect assumption of the viscosity distribution or of the magnitude of the bed shear stress, or it may result from an imperfection of the measurements. The grid configuration effects in the bend restrict the accuracy of the computation of the secondary flow near the sides of the flume. Because of the narrowness of the DHL- flume the accuracy of the computation of the secondary flow in a relatively large part of the flow is affected. For the computation of the secondary flow in a tidal channel the effect will be much less important.

References

1. Booij, N. and de Boer, S., 1981, User's guide for the program TIDES for two-dimensional tidal computations, Delft Univ. of Techn., Dept. of Civil Engrg.
2. Booij, R., 1983, discussion to: Vreugdenhil, C.B. and Wijbenga, J.H.A., Computation of flow patterns in rivers, J. Hydr. Div. ASCE, to be published.
3. Booij, R. and Kalkwijk, J.P.Th., 1982, Secondary flow in Estuaries due to the Curvature of the Main Flow and to the Rotation of the Earth and its Development, Delft Univ. of Techn., Dept. of Civil Engrg., Lab. of Fluid Mech., report 9 - 82.
4. Fischer, H.B. et al., 1979, Mixing in Inland and coastal waters, New York, Academic Press.
5. Flokstra, C., 1976, Generation of two-dimensional horizontal secondary currents, Delft Hydr. Lab., Research report, S163 part II.
6. Kalkwijk, J.P.Th. and de Vriend, H.J., 1980, Computation of the flow in shallow river bends, Journal of Hydraulic Research 18, no. 4.
7. Kuipers, J. and Vreugdenhil, C.B., 1973, Calculations of two-dimensional horizontal flow, Delft Hydr. Lab., Report on basic research, S163 part I.
8. Leendertse, J.J., 1967, Aspects of a Computational Model for Long Period Water Wave Propagation, Memorandum, RM-5294-pr, Rand Corp., Santa Monica, Calif.
9. Olesen, K.W., 1982, Introduction of streamline curvature into flow computation for shallow river bends, Delft Univ. of Techn., Dept. of Civil Engrg., Lab. of Fluid Mech., report no. 5 -82.
10. Pennekamp, Joh.G.S. and Booij, R., 1983, Simulation of flow in rivers and tidal channels with an implicit finite difference method of the ADI-type, Delft Univ. of Techn., Dept. of Civil Engrg., Lab. of Fluid Mech., report no. 3 -83.
11. Stelling, G.S., 1983, Thesis, Delft Univ. of Techn., to be published.
12. Vreugdenhil, C.B. and Wijbenga, J.H.A., 1982, Computation of Flow Patterns in Rivers, ASCE-proc., 108, no. HY 11.
13. Vriend, H.J. de , 1976, A mathematical model of steady flow in curved shallow channels, Comm. on Hydraulics, Delft Univ. of Techn., report no. 76 - 1.

14. Vriend, H.J. de, 1981, Steady flow in shallow channel bends, Thesis, Delft Univ. of Techn.; Comm. on Hydraulics, Delft Univ. of Techn., report no. 81 -3.

15. Vriend, H.J. de and Koch, F.G., 1977, Flow of water in a curved open channel with a fixed plane bed, TOW, Report on experimental and theoretical investigations, R657-V, M 1415 part I.

16 Vriend, H.J. de and Koch, F.G., 1978, Flow of water in a curved open channel with a fixed uneven bed, TOW, Report on experimental and theoretical investigations, R657-VI, M 1415 part II.

17. Weare, T.J., 1979, Errors arising from irregular boundaries in ADI solutions of the shallow water equations, Int. J. Num. meth. Eng., vol. 14, pp. 921-931.

Notation

B	width of the flume
c_b	coefficient in the secondary flow intensity
C	Chézy coefficient
$f_b, f_c,$	form funtions of the secondary flow components
g	acceleration due to gravity
h	depth of flow
$i, i+1$, etc	subscript indicating the grid point number
I_n	secondary flow intensity
n	(local) flow coordinate perpendicular to the direction of the depth averaged flow
r	distance to the center of curvature of the flume
R	radius of curvature of the main flow
R_f	radius of curvature of the channel axis
s	(local) flow coordinate in the direction of the depth averaged flow
t	time
T_{xx}, T_{xy}, T_{yy}	effective stresses in vertical planes
u	depth averaged velocity in x-direction
u_n	secondary flow velocity
u_s	main flow velocity; depth averaged velocity
$\bar{u}_s$	depth averaged velocity
u_n^b, u_n^c	velocity of the secondary flow components
u_*	friction velocity
v	depth averaged velocity in y-direction
x	horizontal coordinate
y	horizontal coordinate
z	vertical coordinate
α, α'	degree of development of the secondary flow components
β	constant
Δ	distance between grid points
Δt	numerical time increment
$\Delta h/\Delta s$	surface gradient along the channel axis
ε	imposed diffusion coefficient
ε_p	diffusion coefficient
ζ	water level with respect to a horizontal reference level
θ	local angle between the s - and x - directions

κ	Von Karman's constant
ν_t	lateral eddy viscosity
ρ	mass density
τ_{bx}, τ_{by}	components of the bottom shear stress
τ_{wx}, τ_{wy}	components of the surface shear stress
ϕ	latitude
ω	angular rotation of the earth
Ω	Coriolis parameter

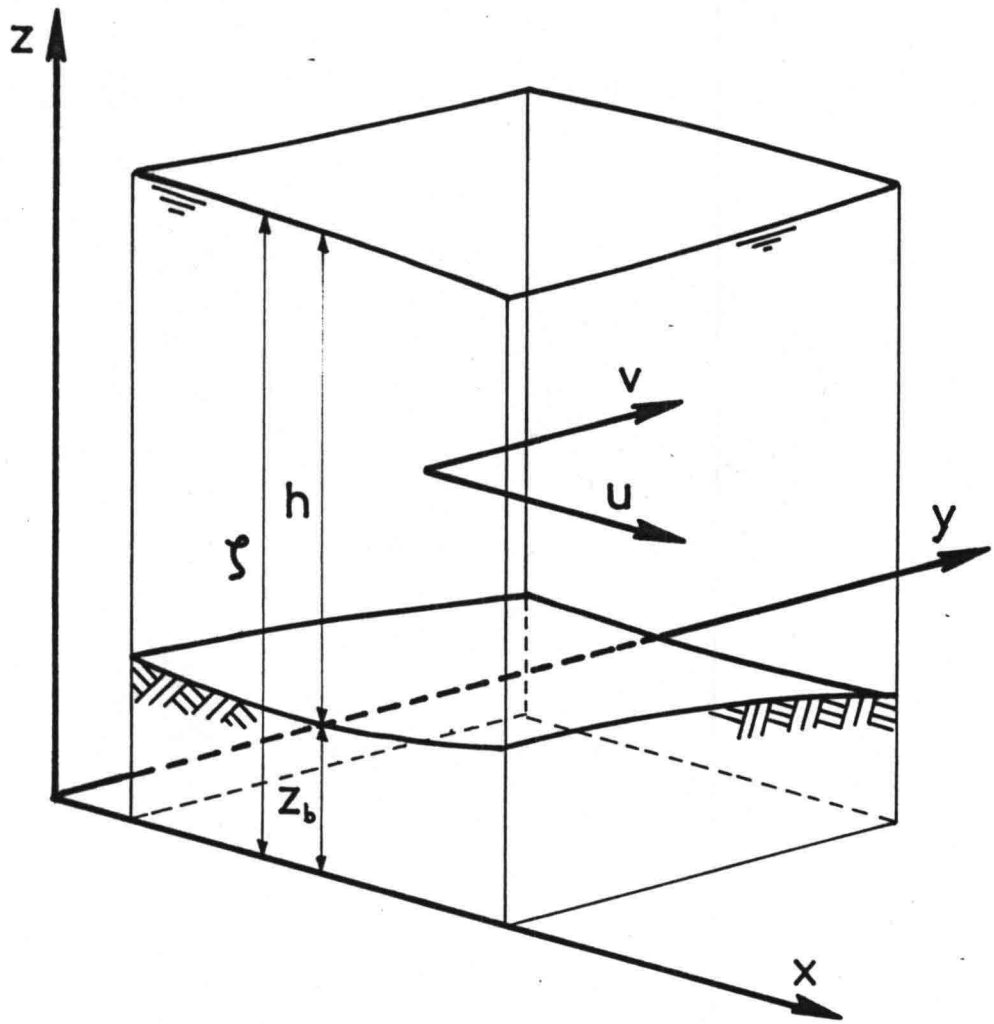

Fig. 1 Definition sketch.

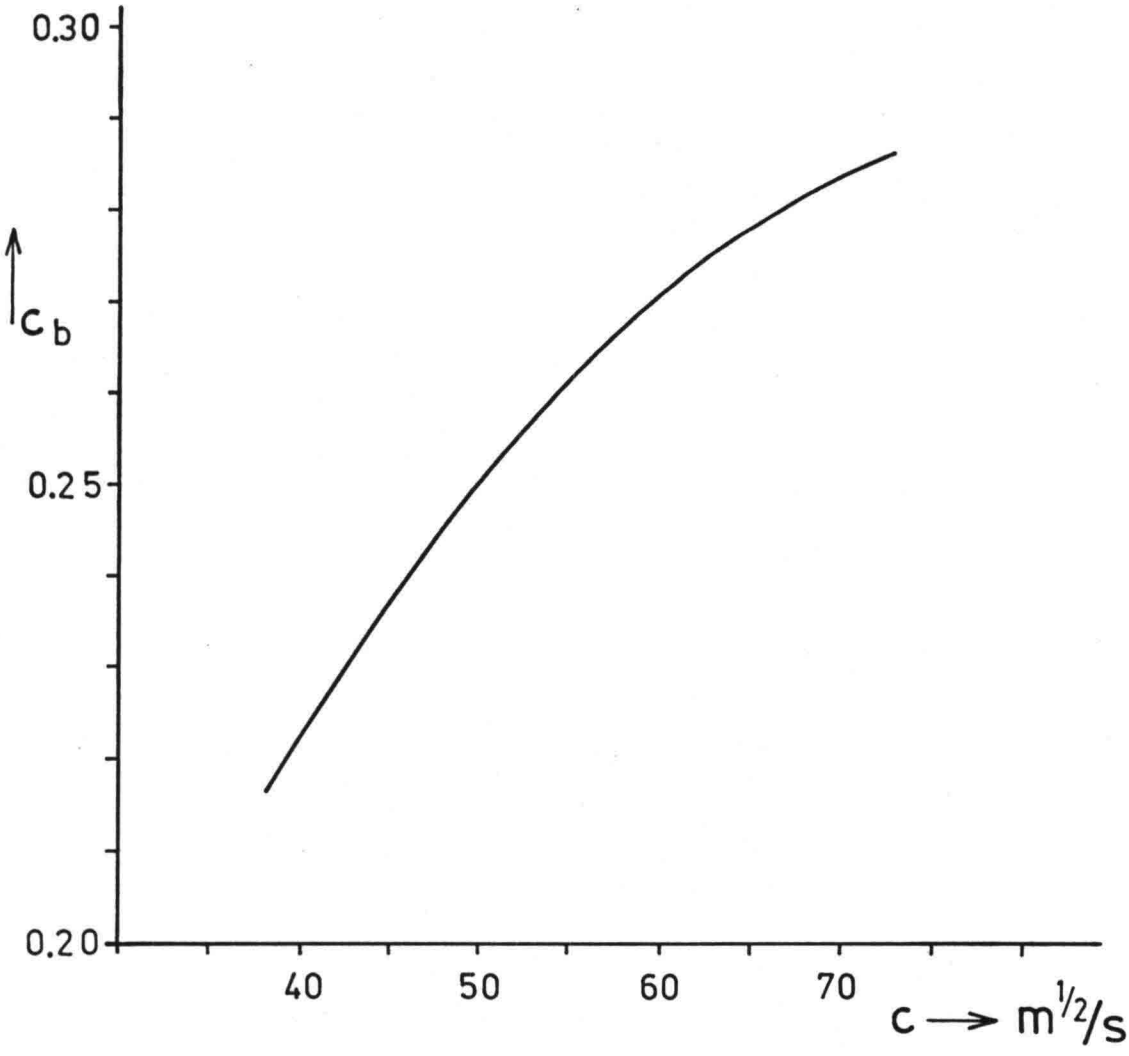

Fig. 2 Relation between the coefficient (c_b) from the intensity expression (Eq. 16) and the Chézy coefficient (C).

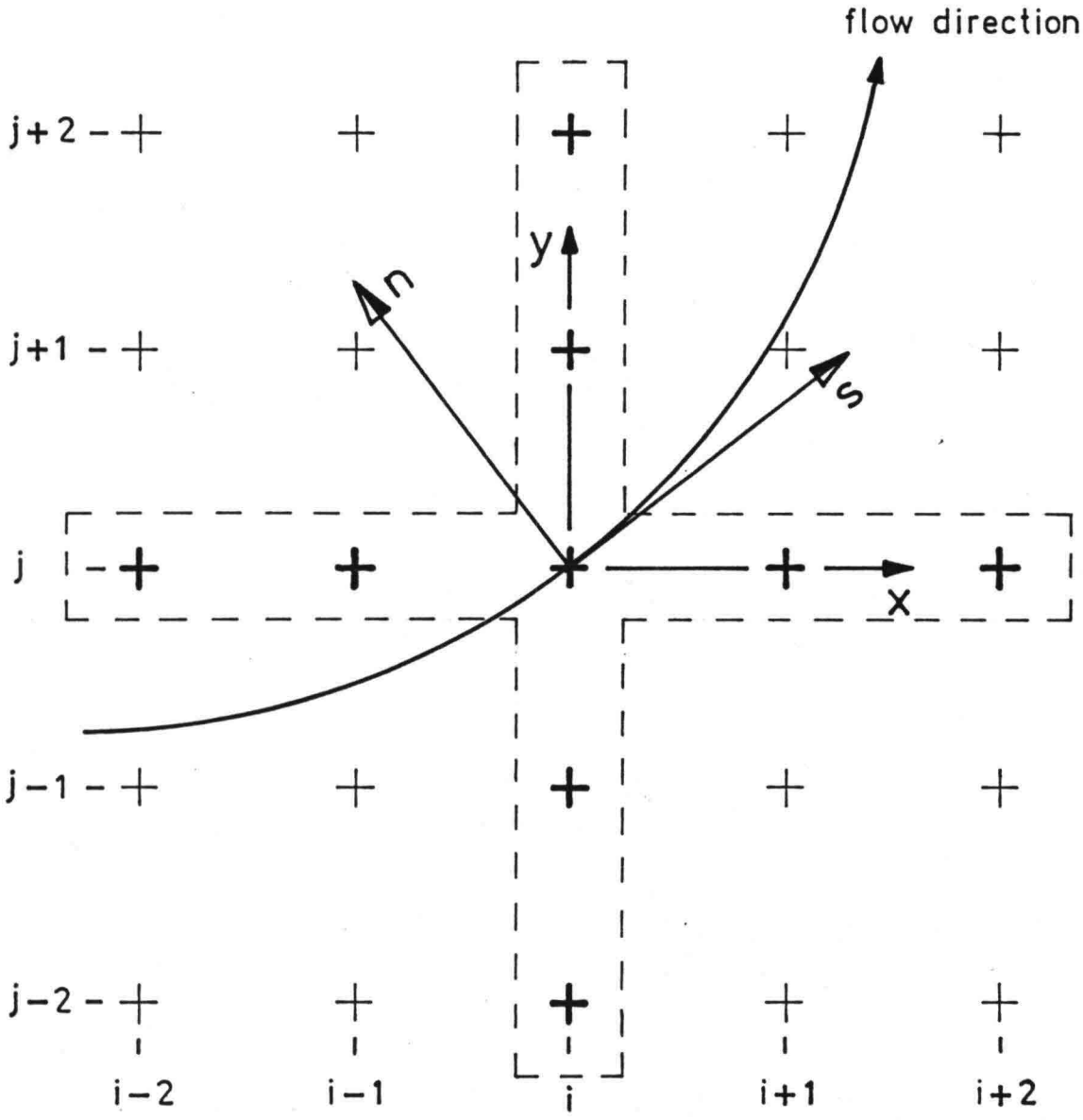

Fig. 3 Difference molecule for the computation of the radius of curvature of the depth averaged flow.

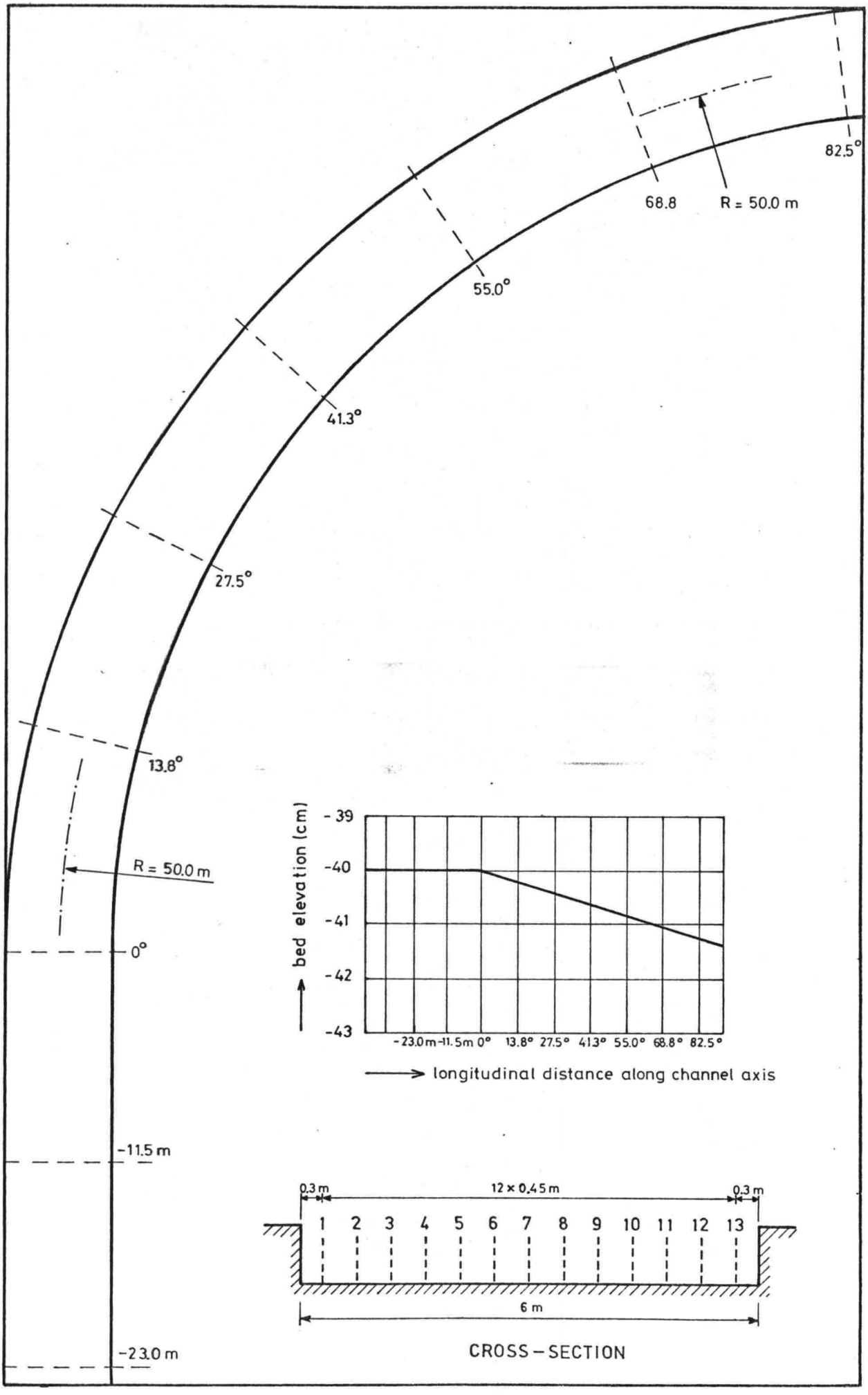

Fig. 4 Geometry of the DHL-flume with the plane bed.

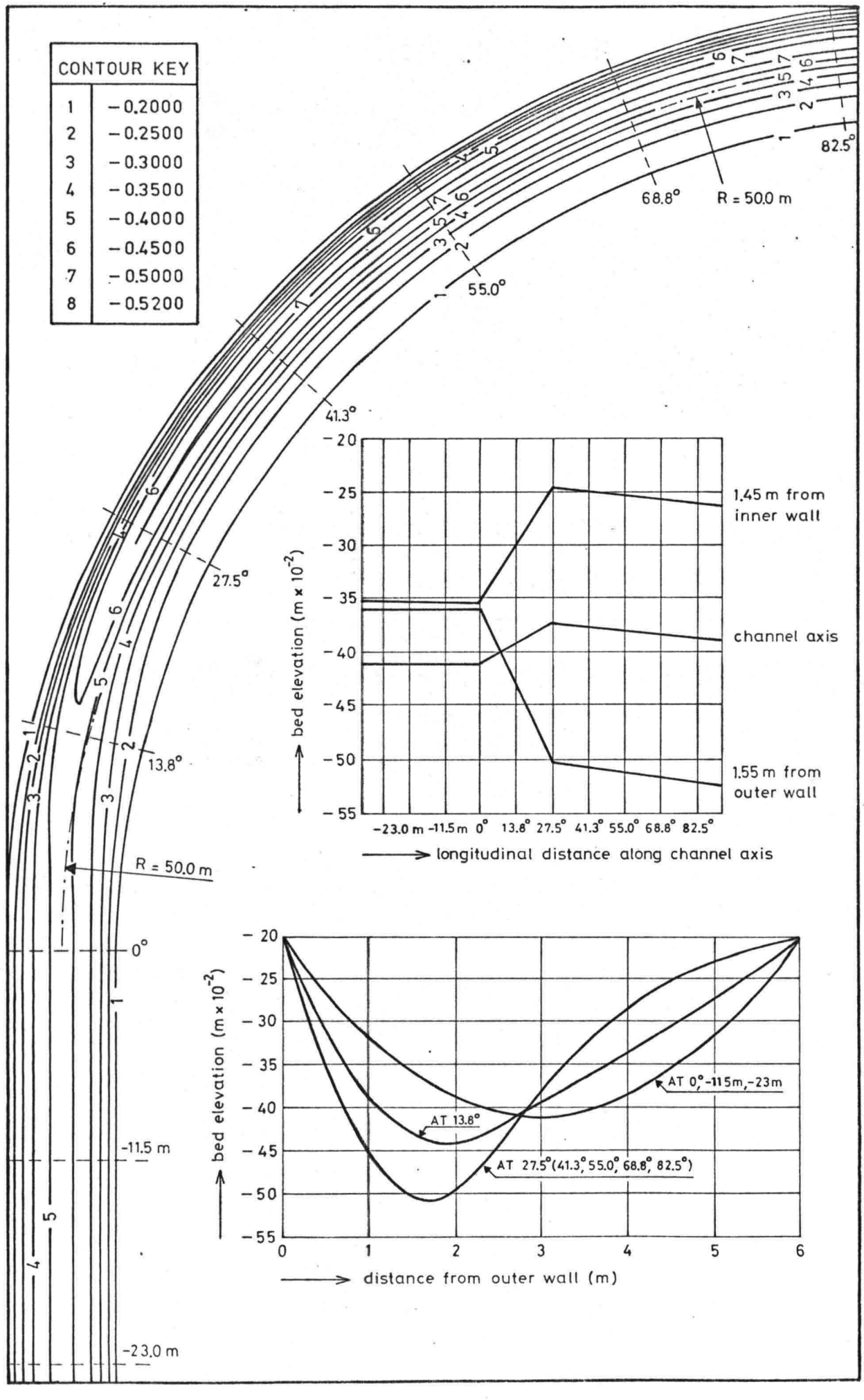

Fig. 5a. Geometry of the DHL-flume with the uneven bed.

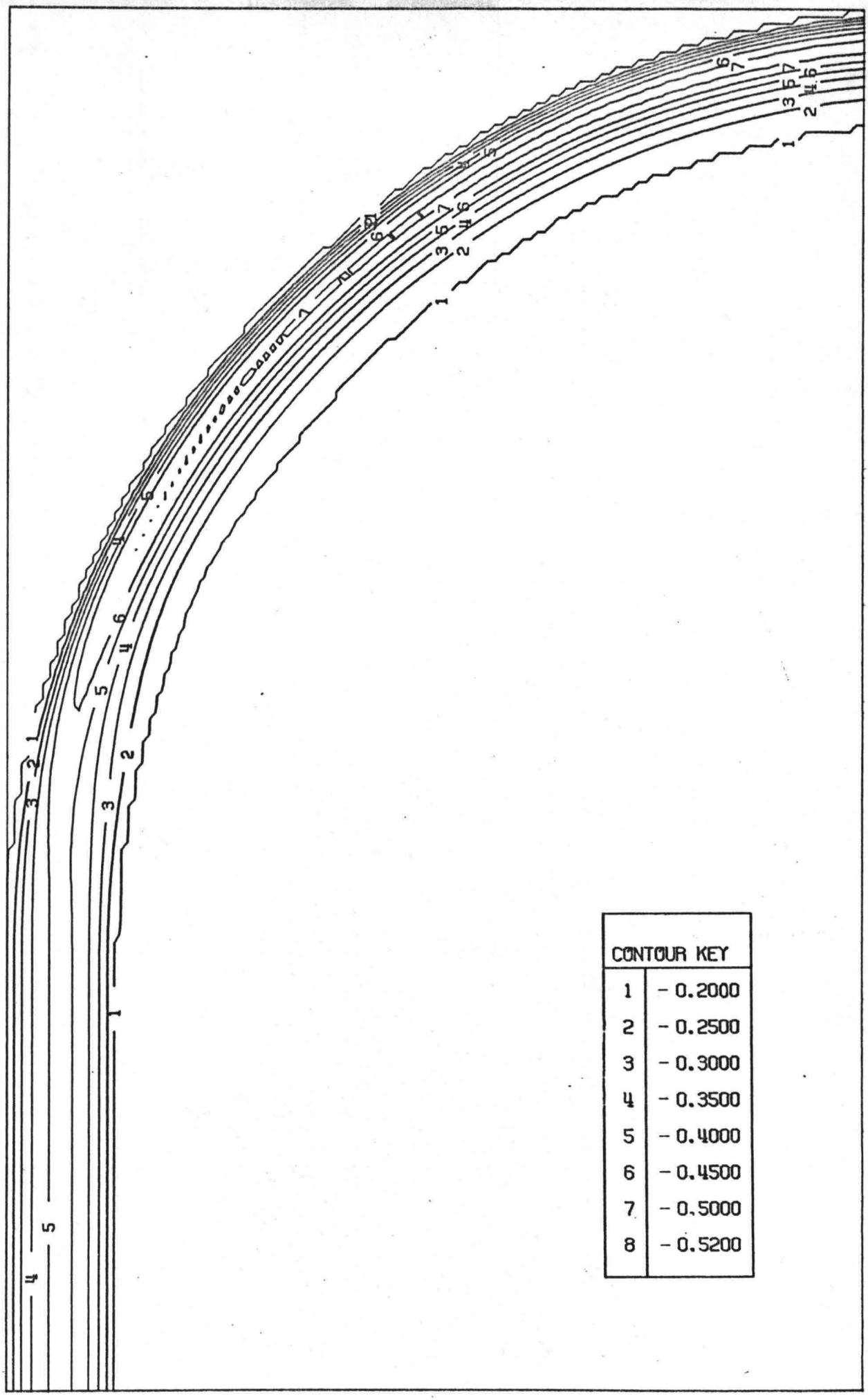

Fig. 5b. Numerical representation of the uneven bed. (depths in m with respect to reference level)

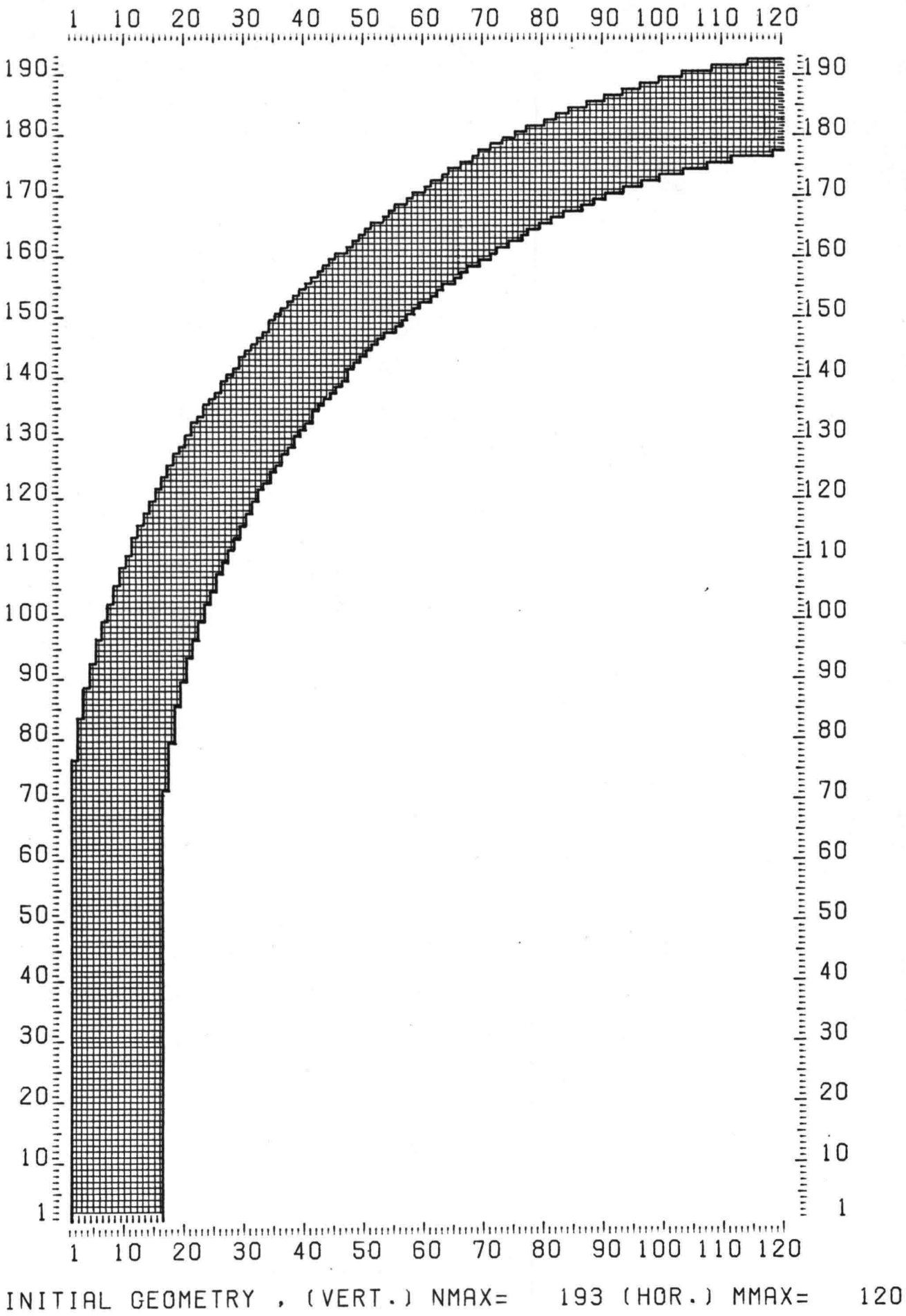

Fig. 6a Computational grid with Δ = 0.40 m.

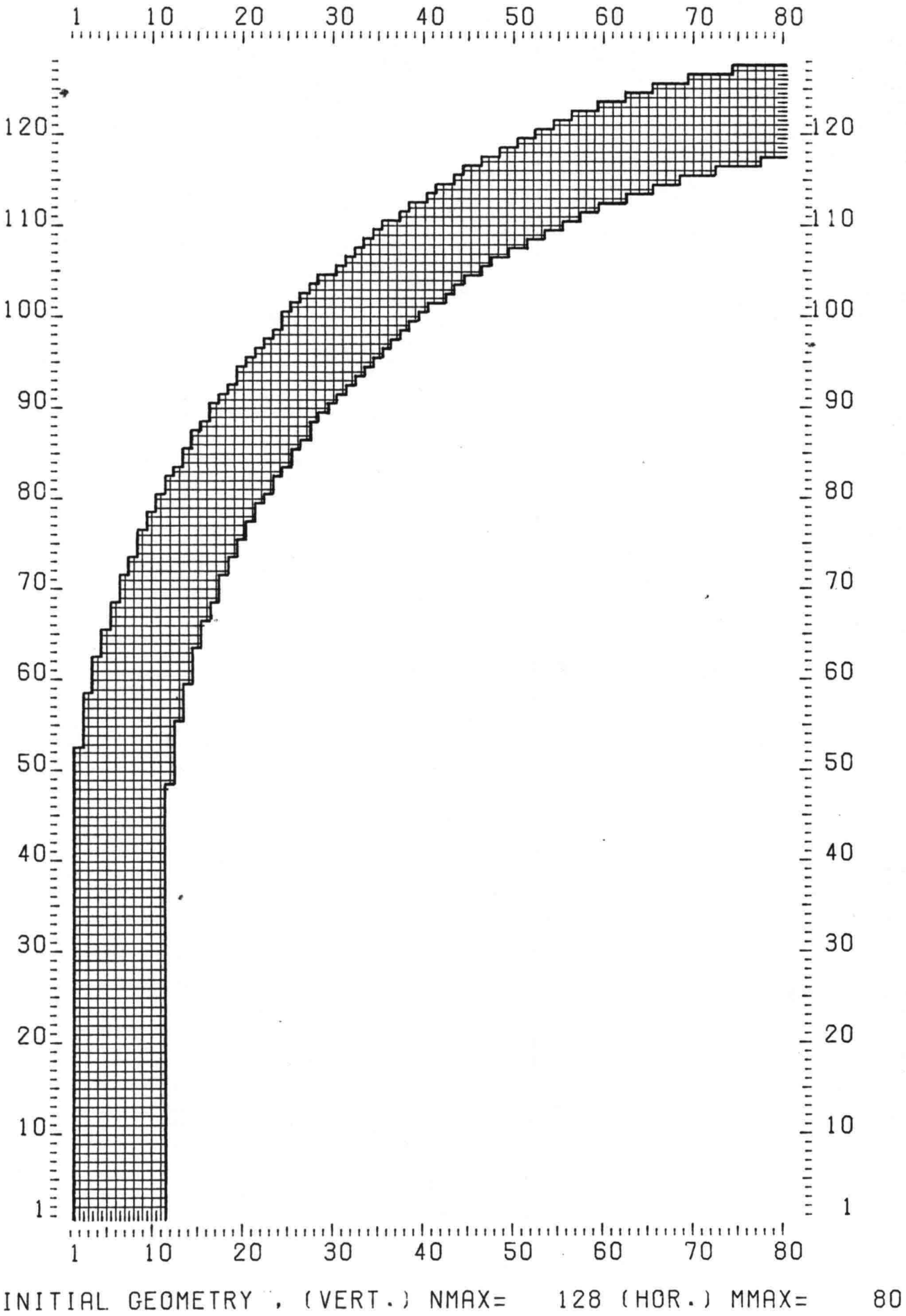

Fig. 6b Computational grid with Δ = 0.60 m.

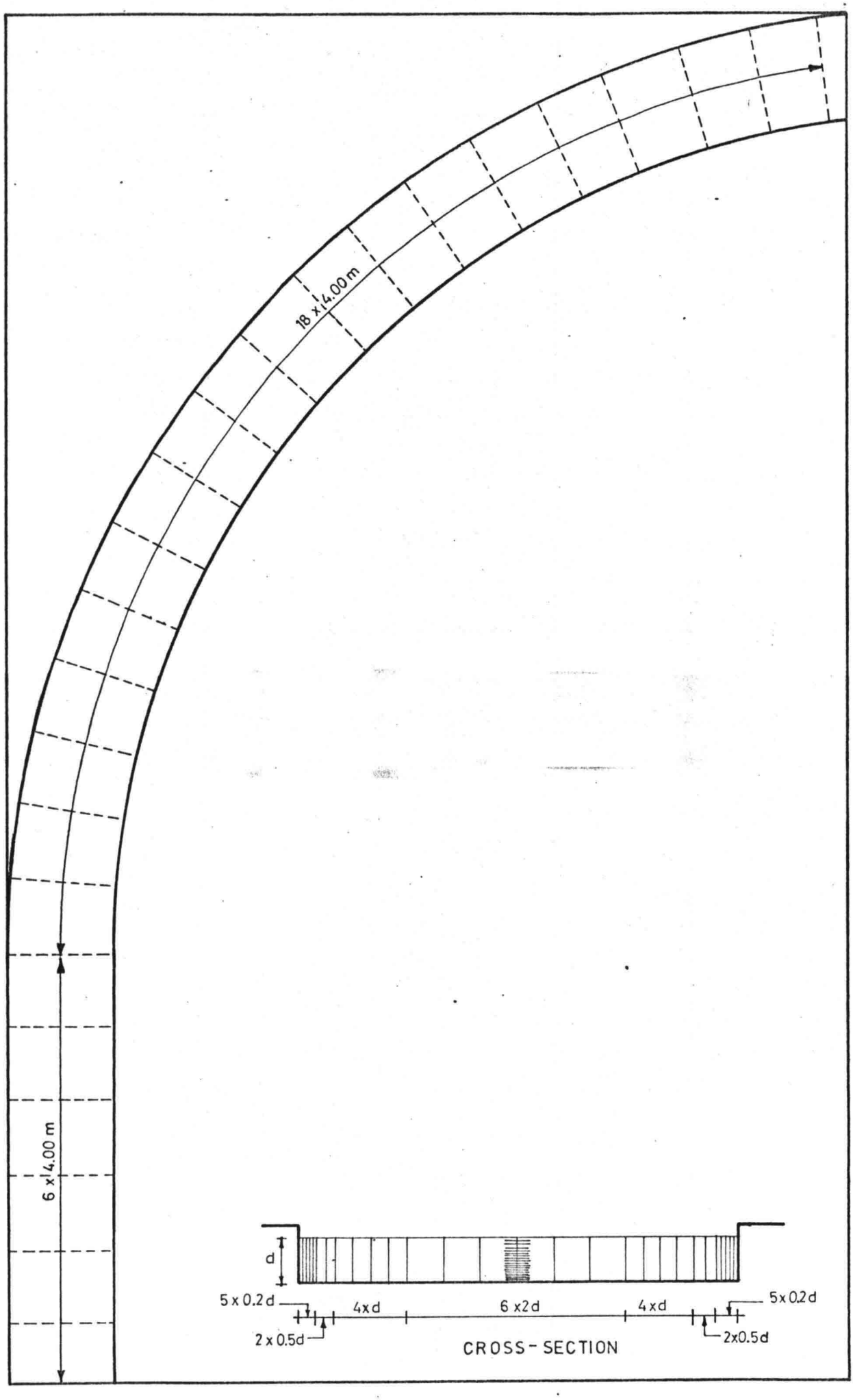

Fig. 7 Computational grid used by de Vriend (1981)

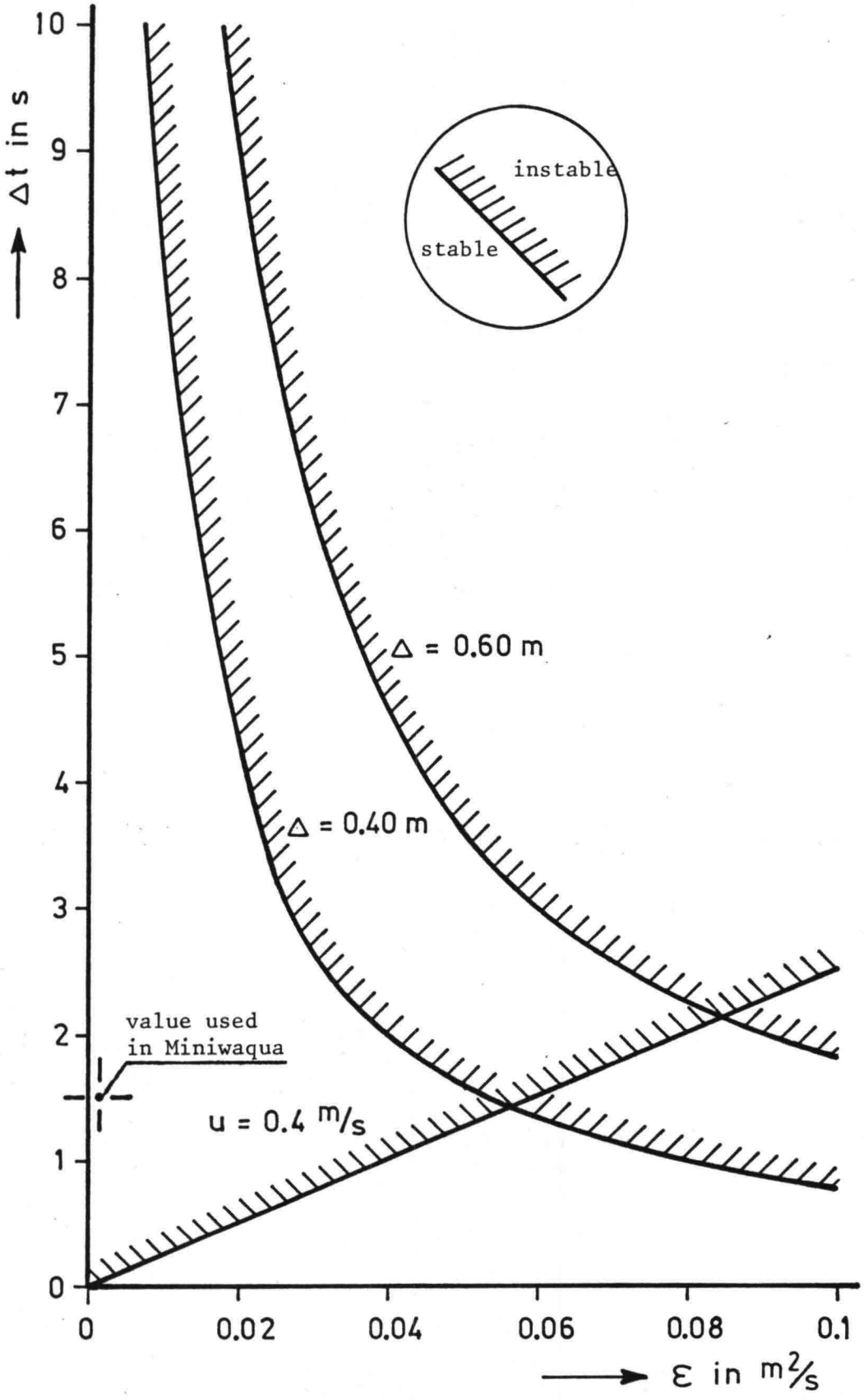

Fig. 8 Stability regions in the $\Delta t - \varepsilon$ plane.

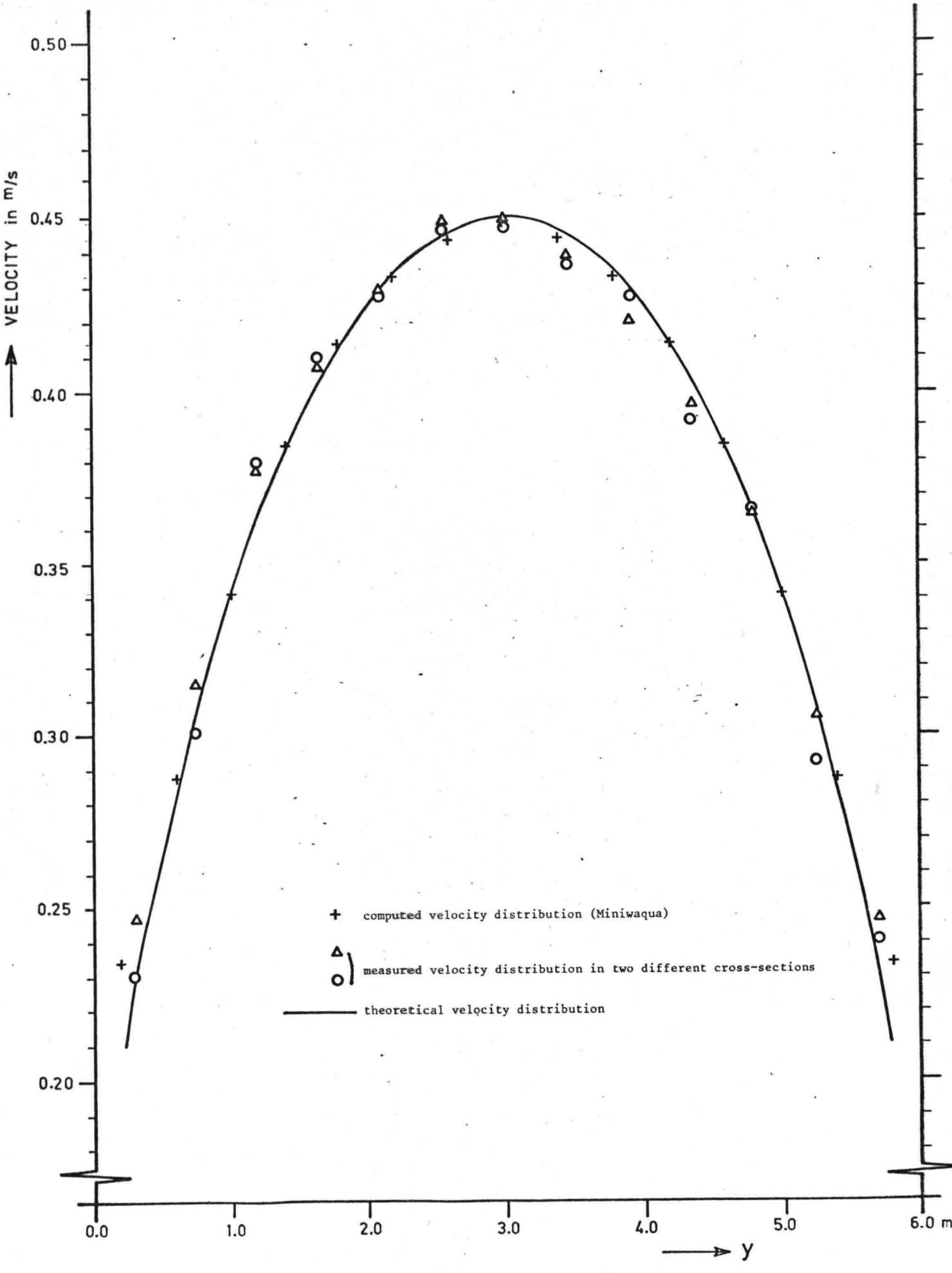

Fig. 9. Depth averaged velocity distribution in the straight part of the DHL-flume. (uneven bed configuration)

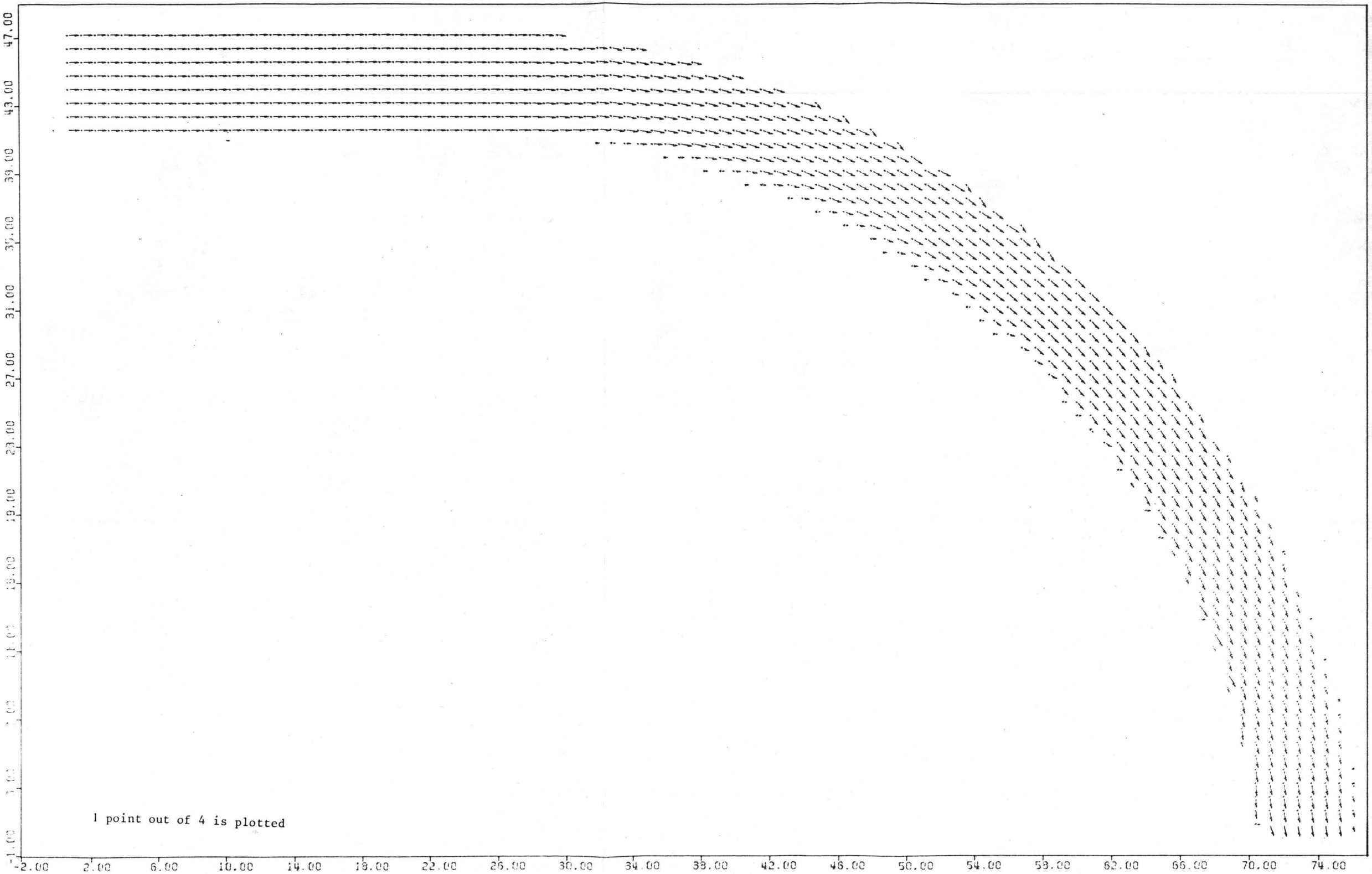

Fig. 10. Depth averaged velocity field (plane bed configuration).

(Vector scale 1 mm = 0.125 m/s)

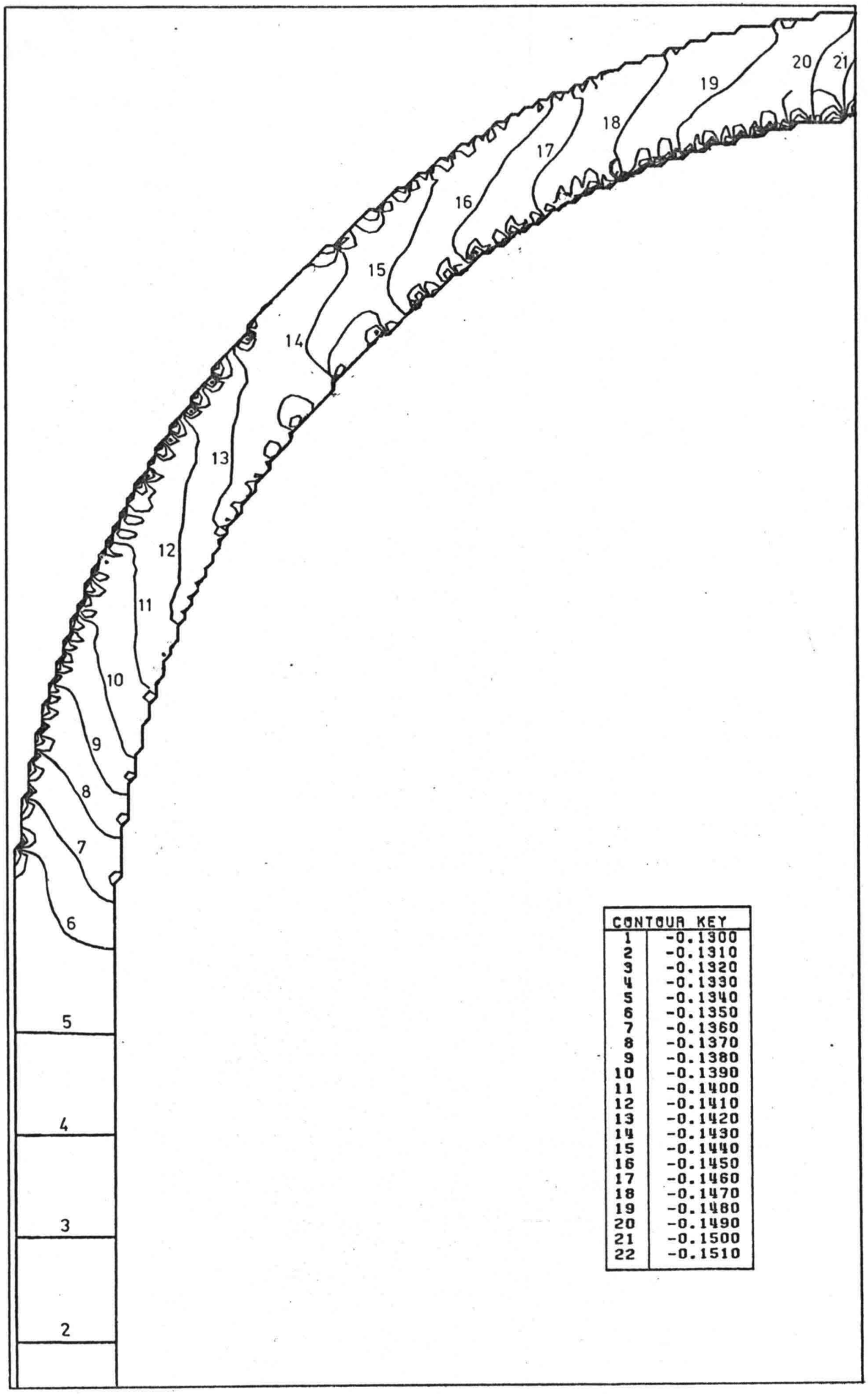

Fig. 11. Surface level contour plot (plane bed configuration).
Heights in m with respect to reference level.

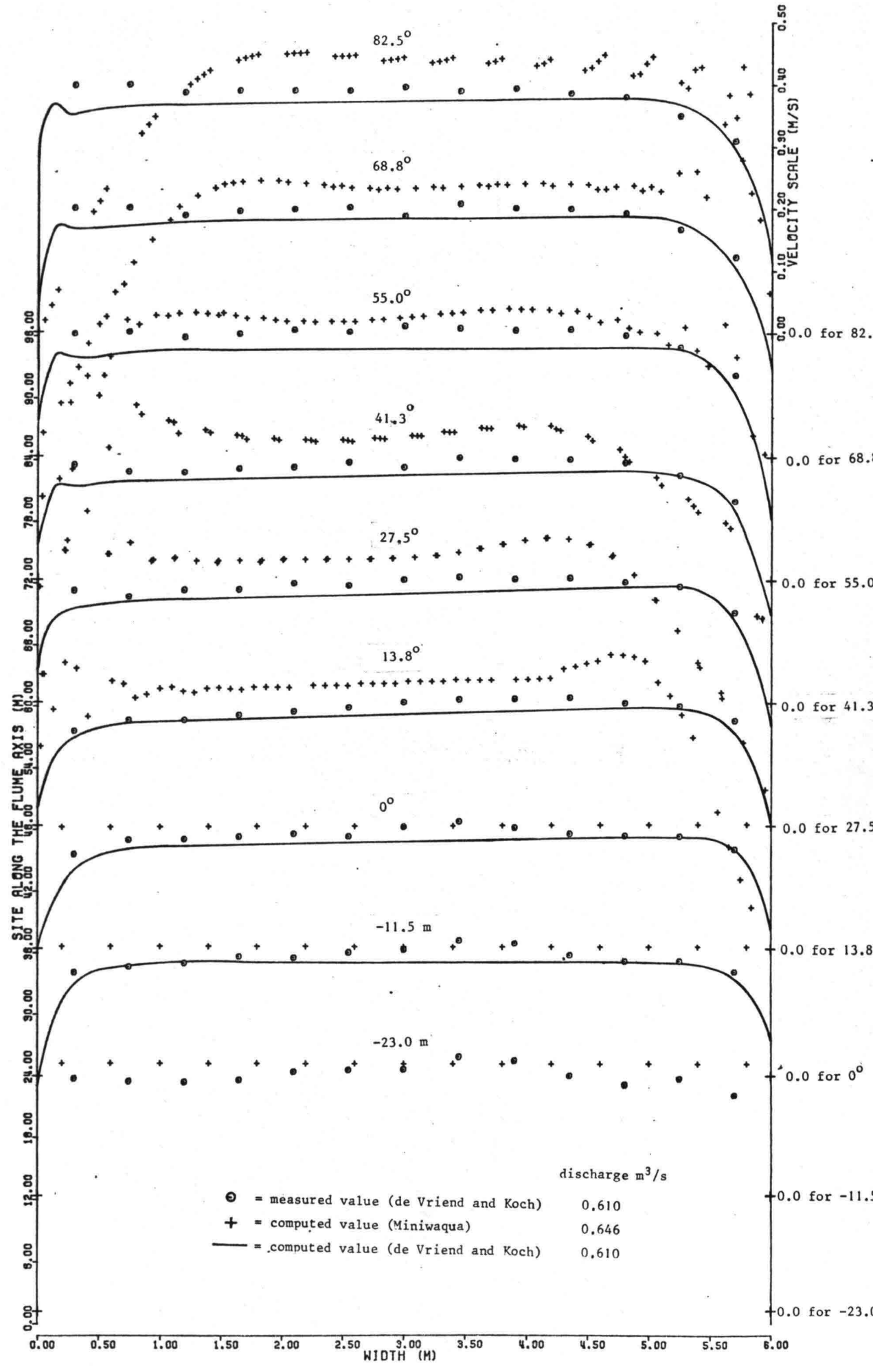

Fig. 12. Depth averaged velocity distributions in several cross-sections (plane bed configuration).

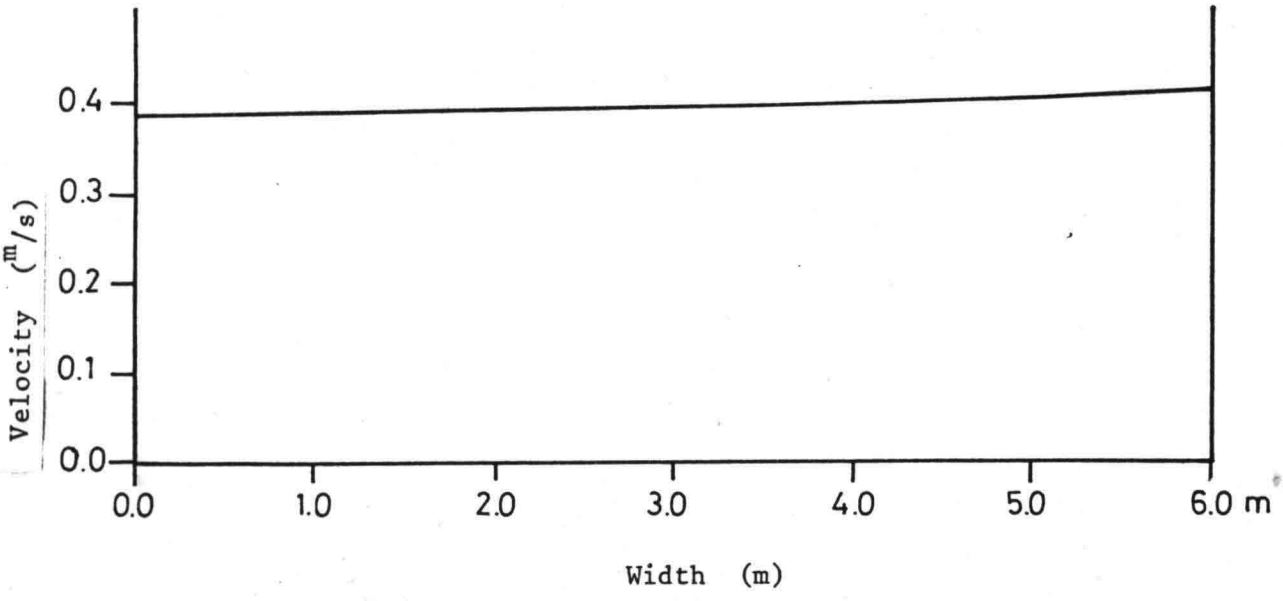

Fig. 13. Equilibrium depth averaged velocity distribution.
(plane bed configuration)

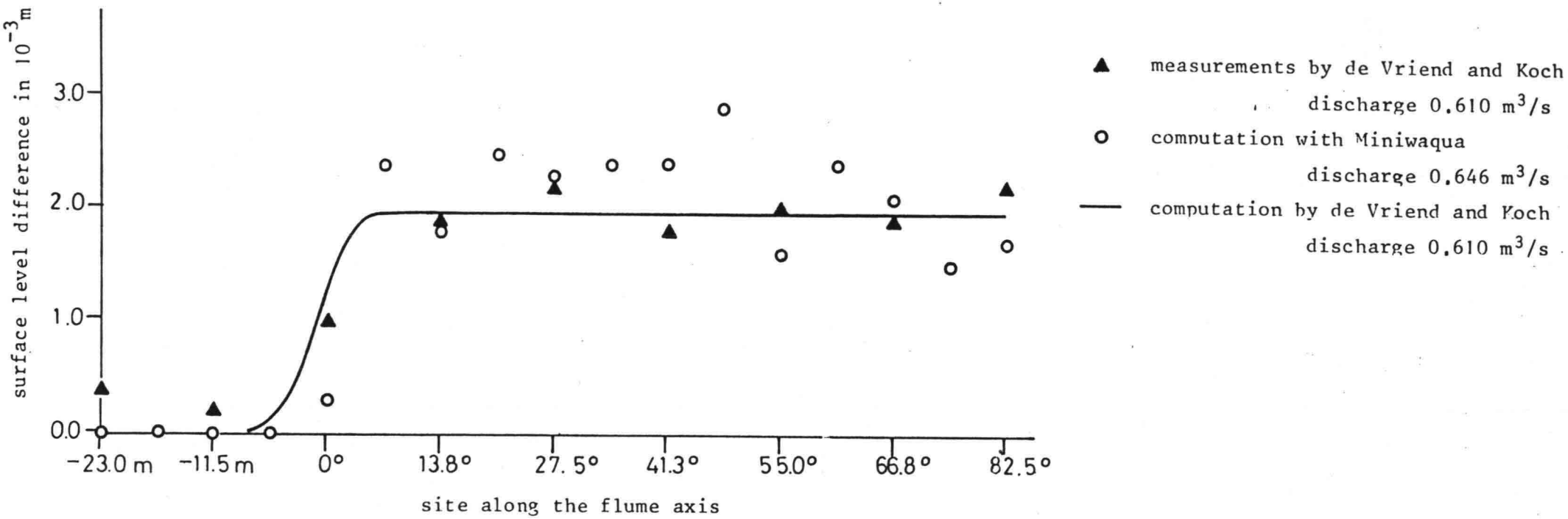

Fig. 14. Transverse surface level difference (plane bed configuration).

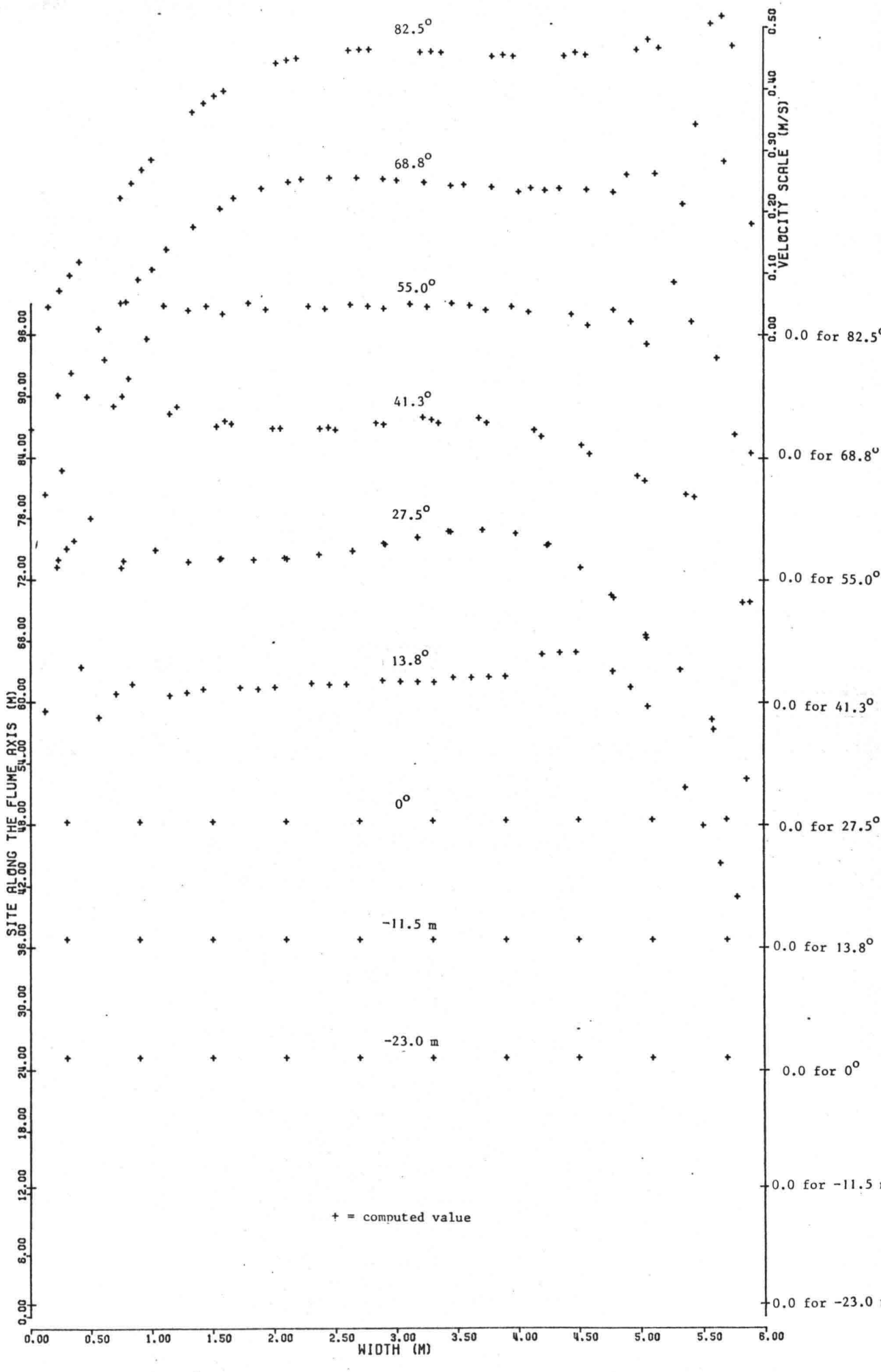

Fig. 15. Depth averaged velocity distributions in several cross-sections (plane bed configuration), $\Delta = 0.60$ m.

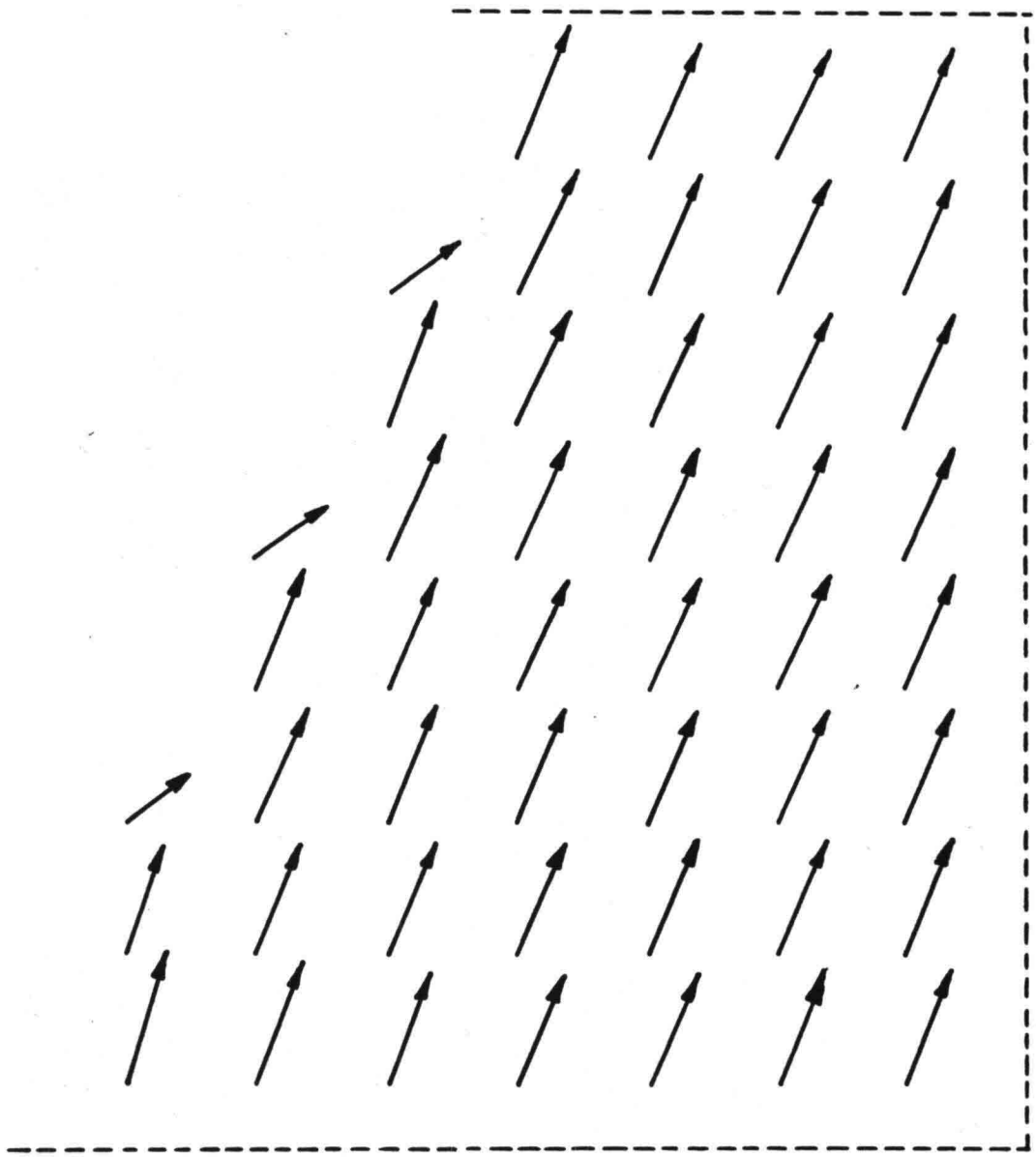

Fig. 16. Obstruction of the flow in the outer bend af 25^{o}.

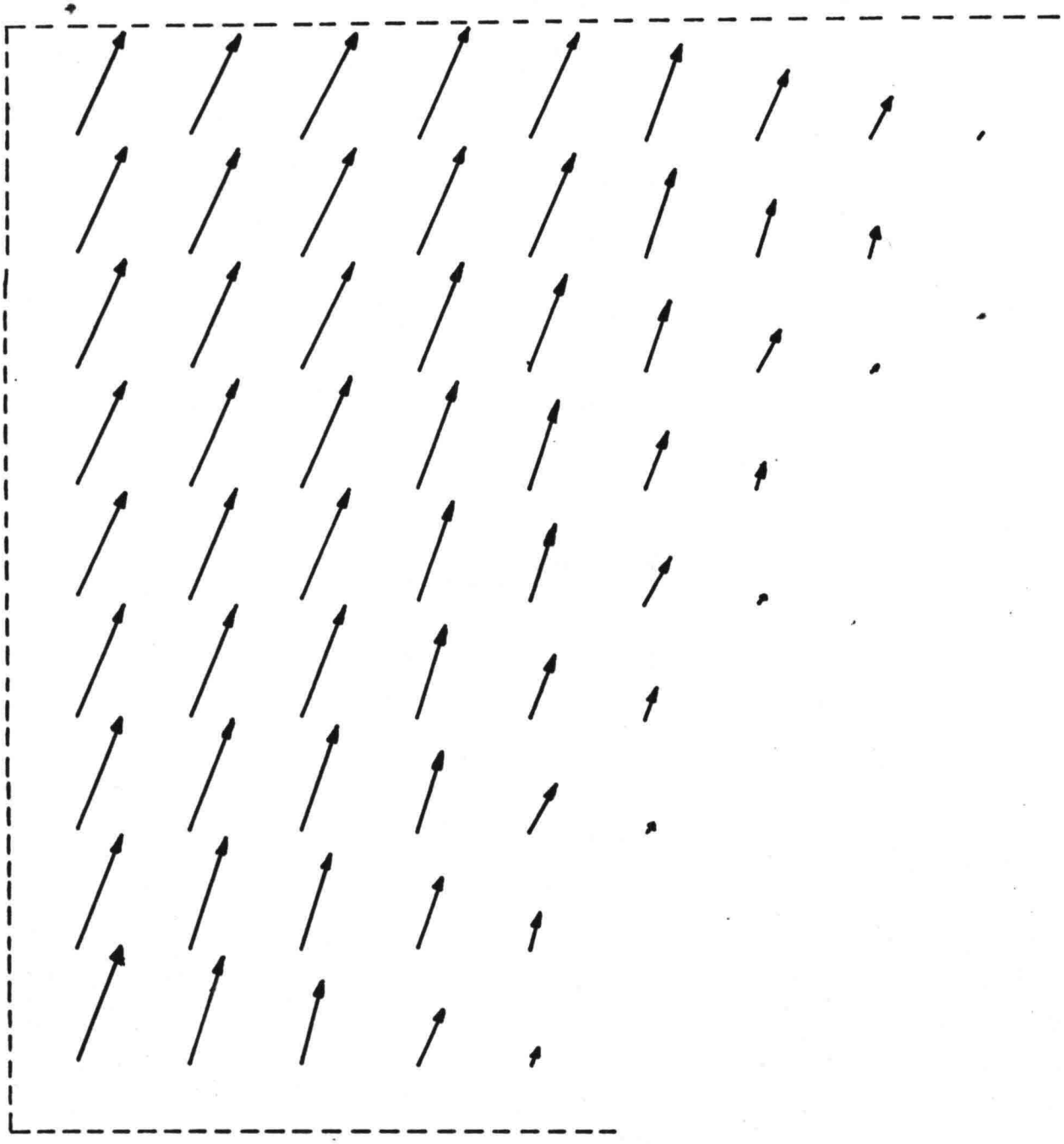

Fig. 17. Widening of the flow in het inner bend at 25°.

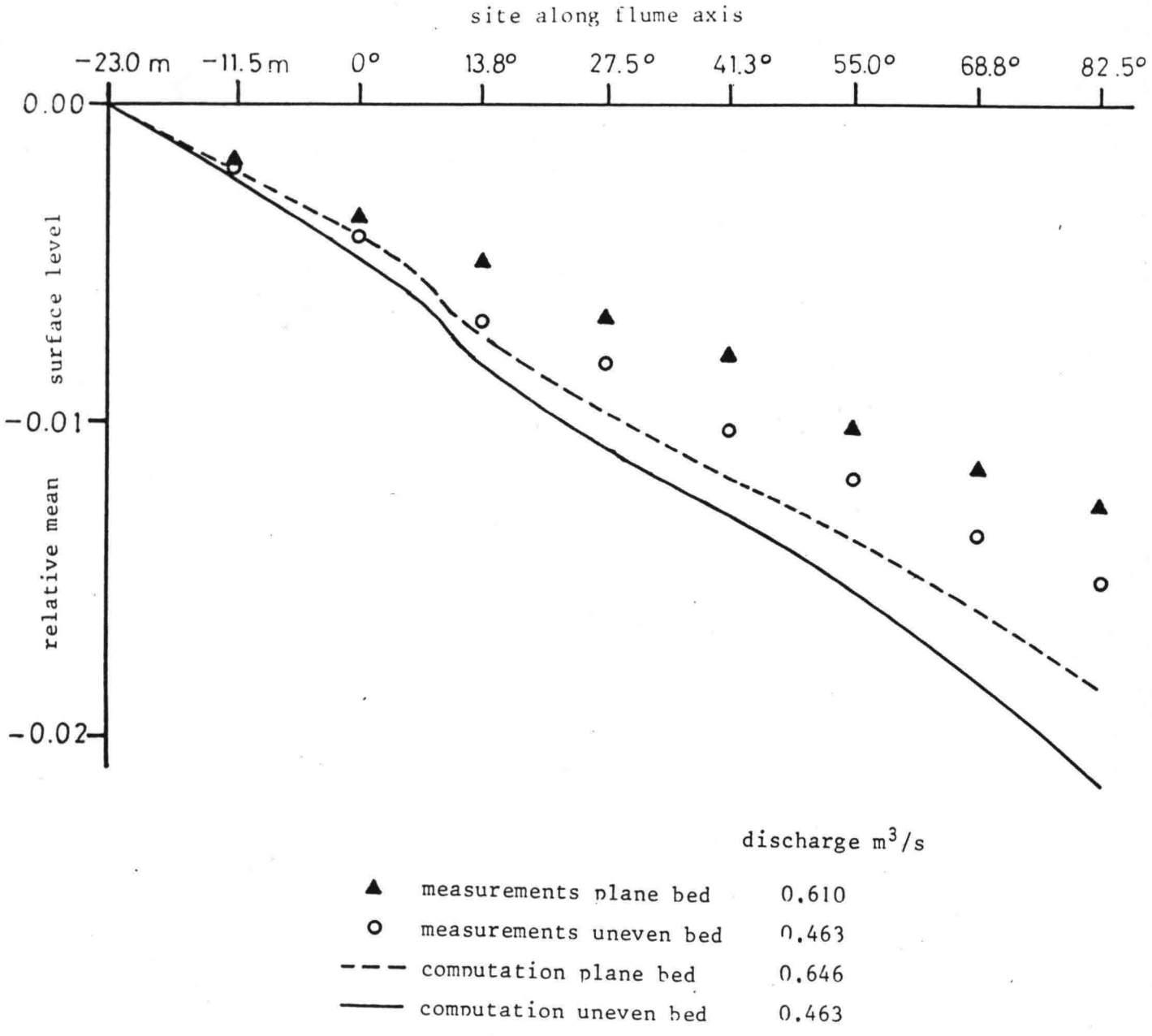

Fig. 18. Longitudinal surface slope.

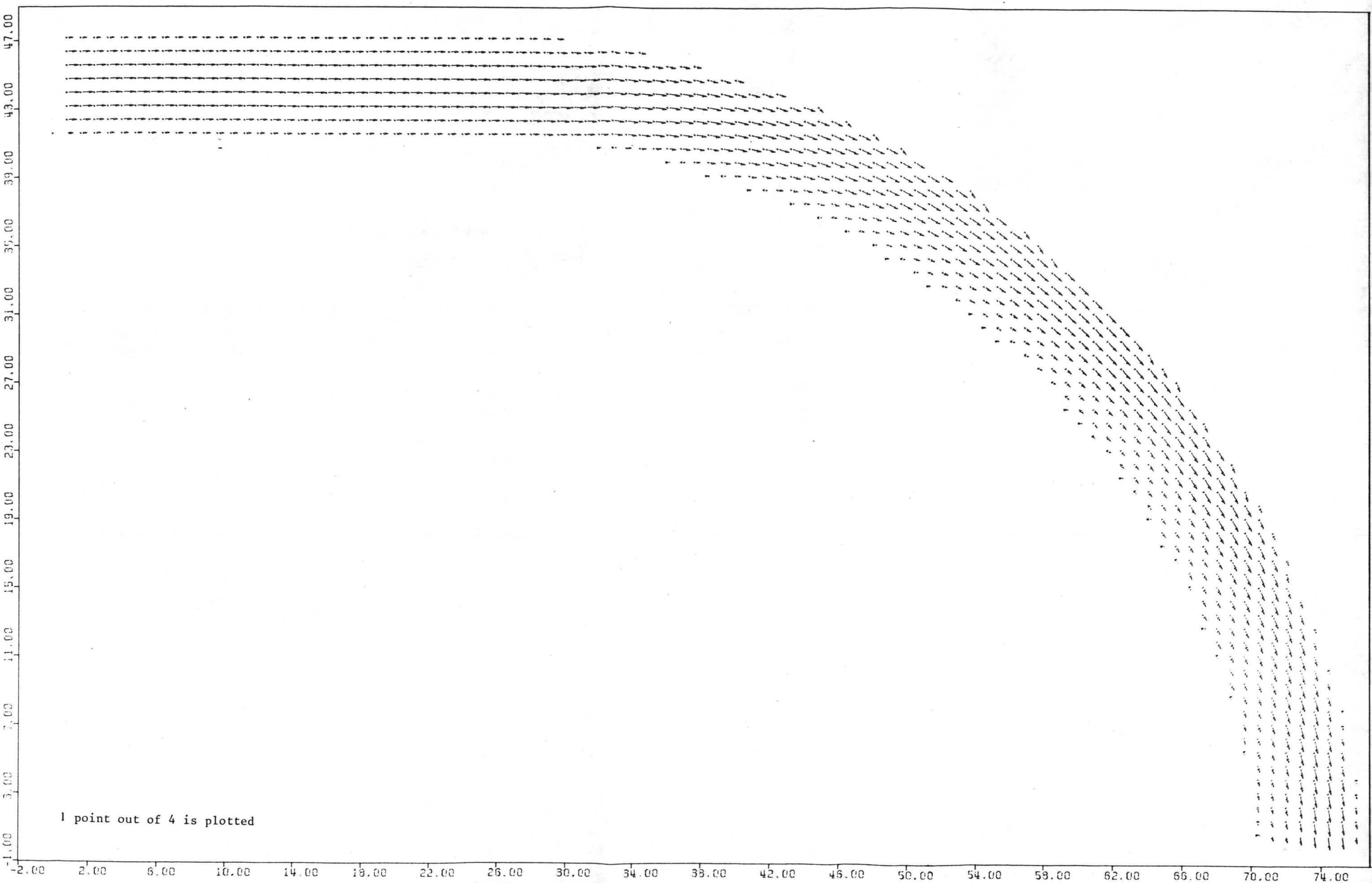

Fig. 19. Depth averaged velocity field (uneven bed configuration).

(Vector scale 1 mm = 0.125 m/s)

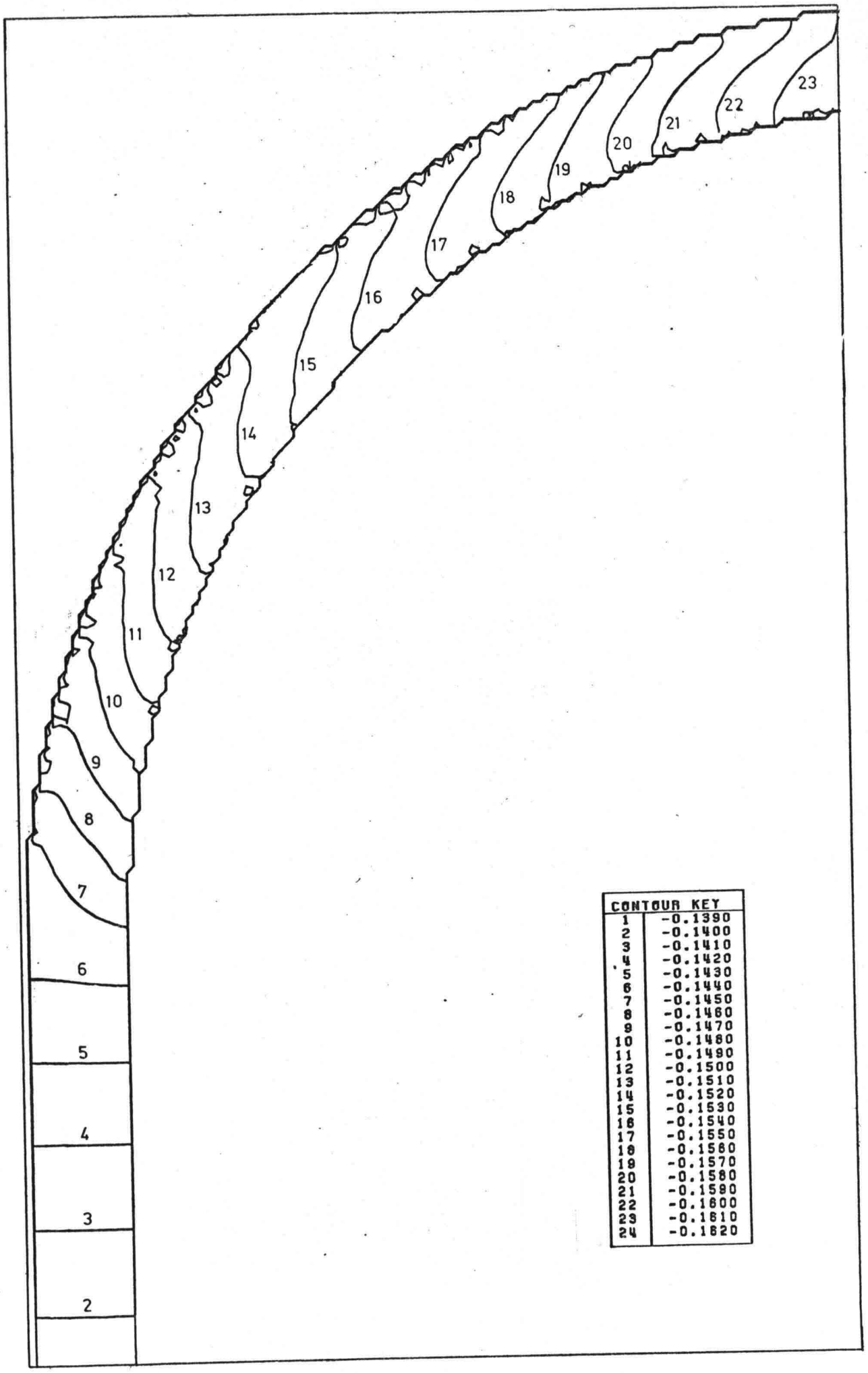

Fig. 20. Surface level contour plot (uneven bed configuration).
Heights in m with respect to reference level.

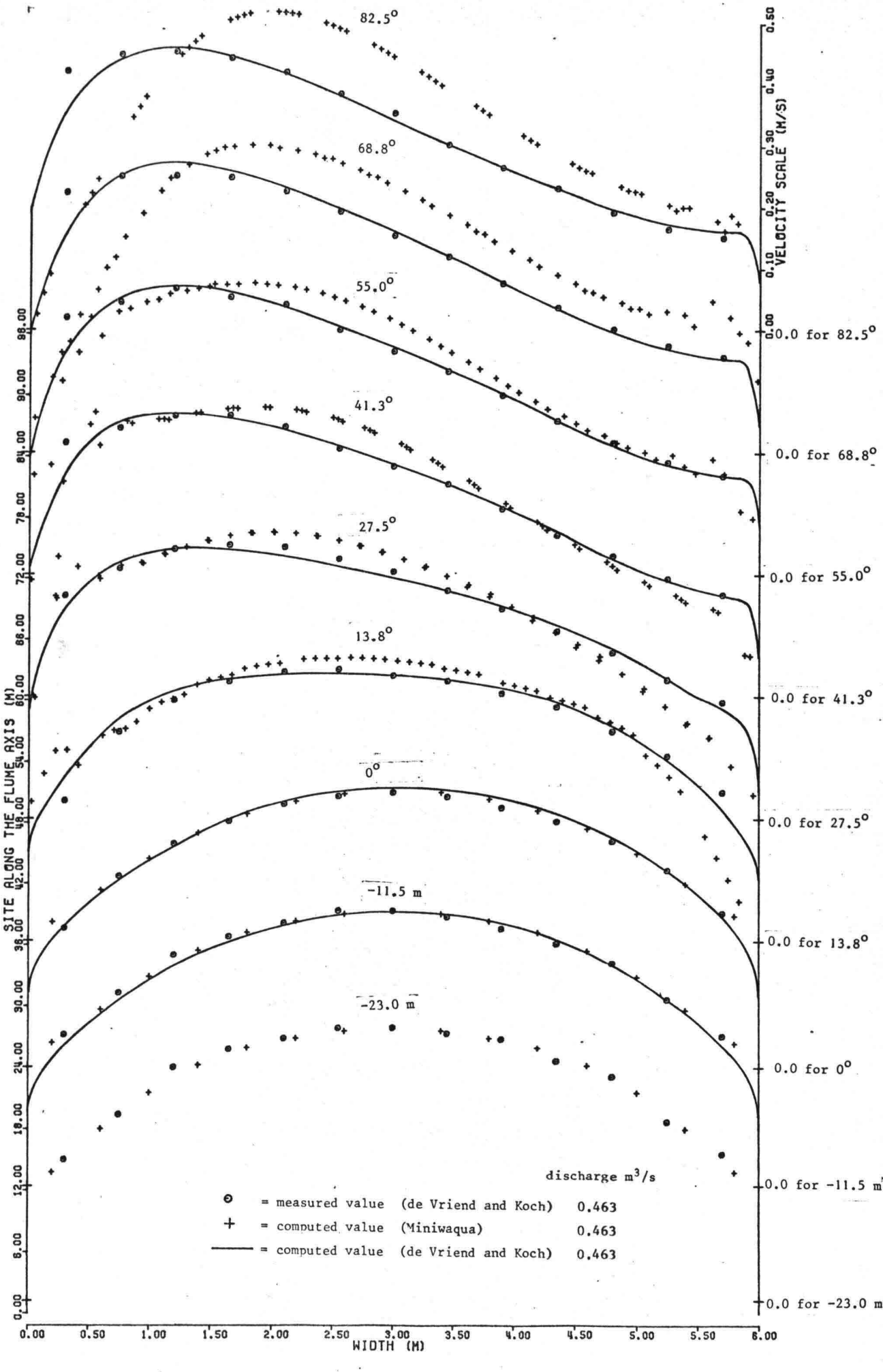

Fig. 21. Depth averaged velocity distributions in several cross-sections (uneven bed configuration).

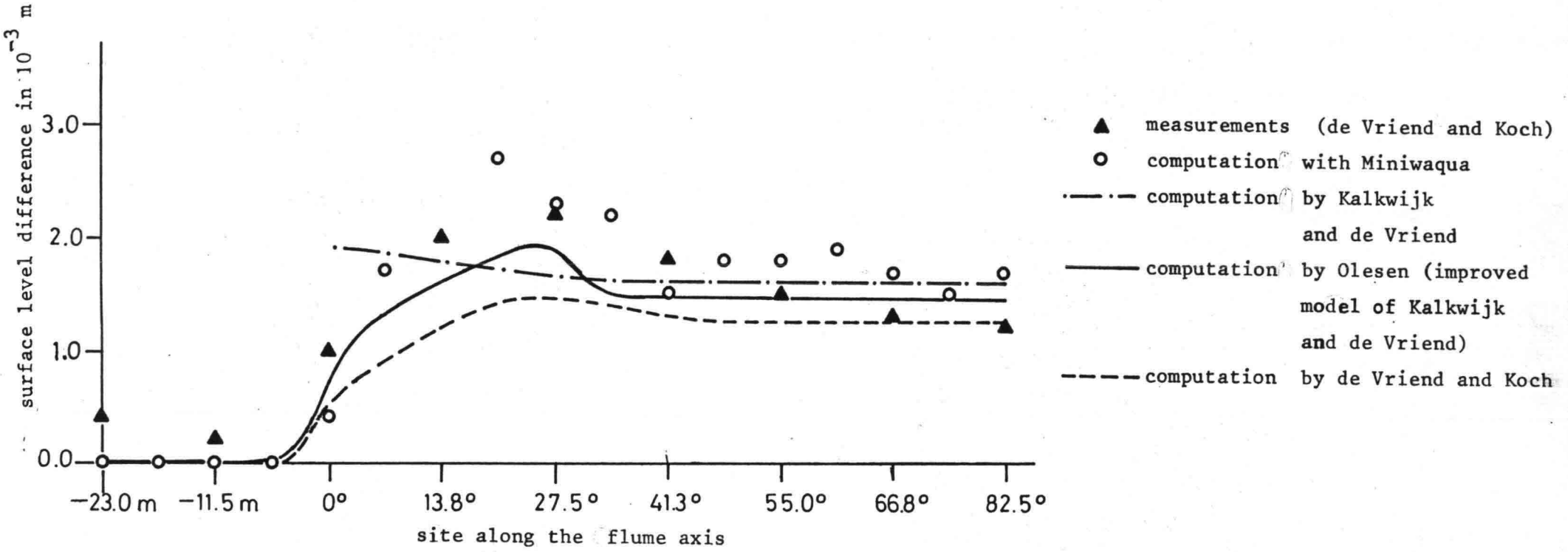

Fig. 22, Transverse surface level difference (uneven bed configuration).

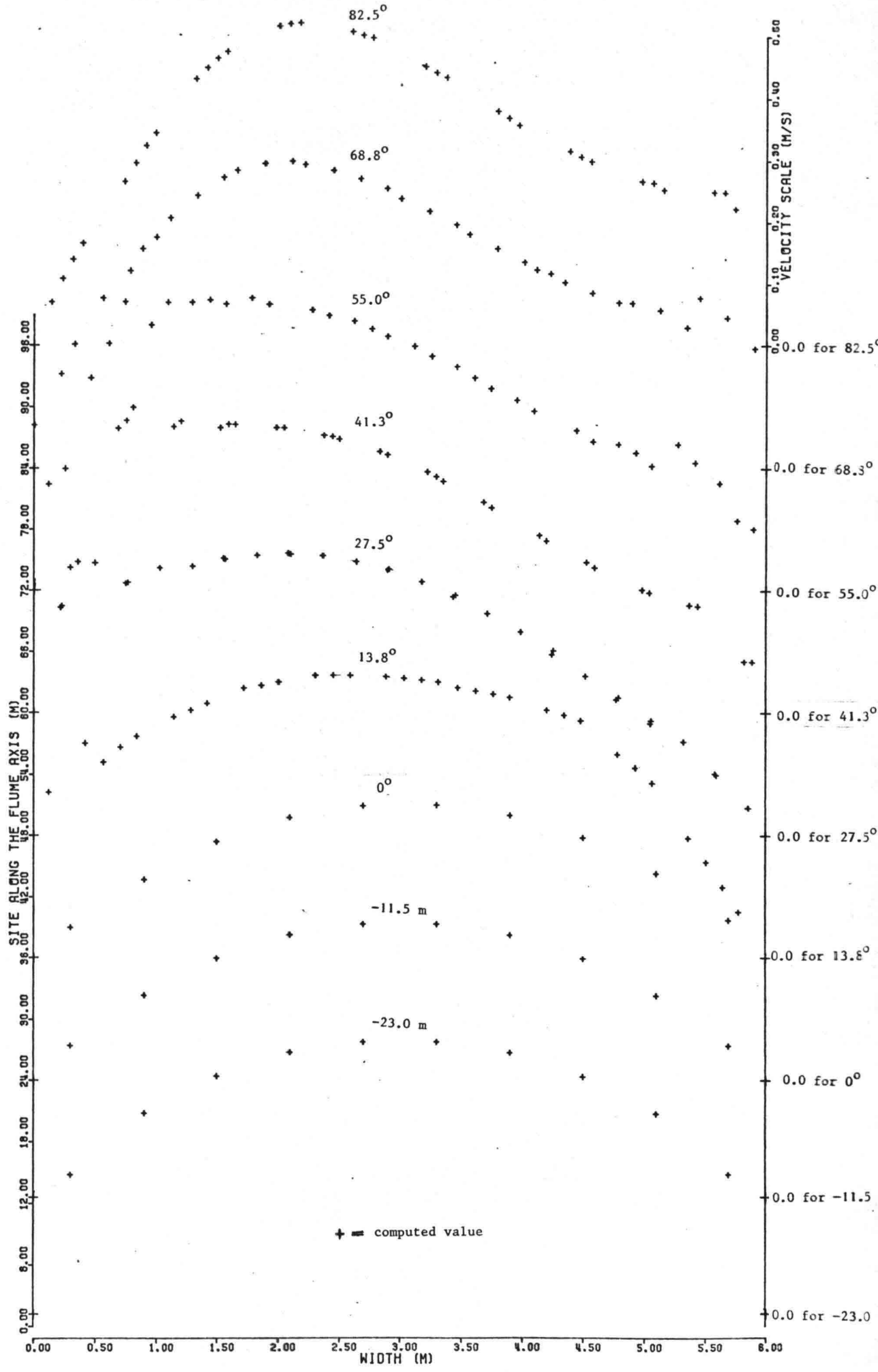

Fig. 23. Depth averaged velocity distributions in several cross-sections (uneven bed configuration), Δ = 0.60 m.

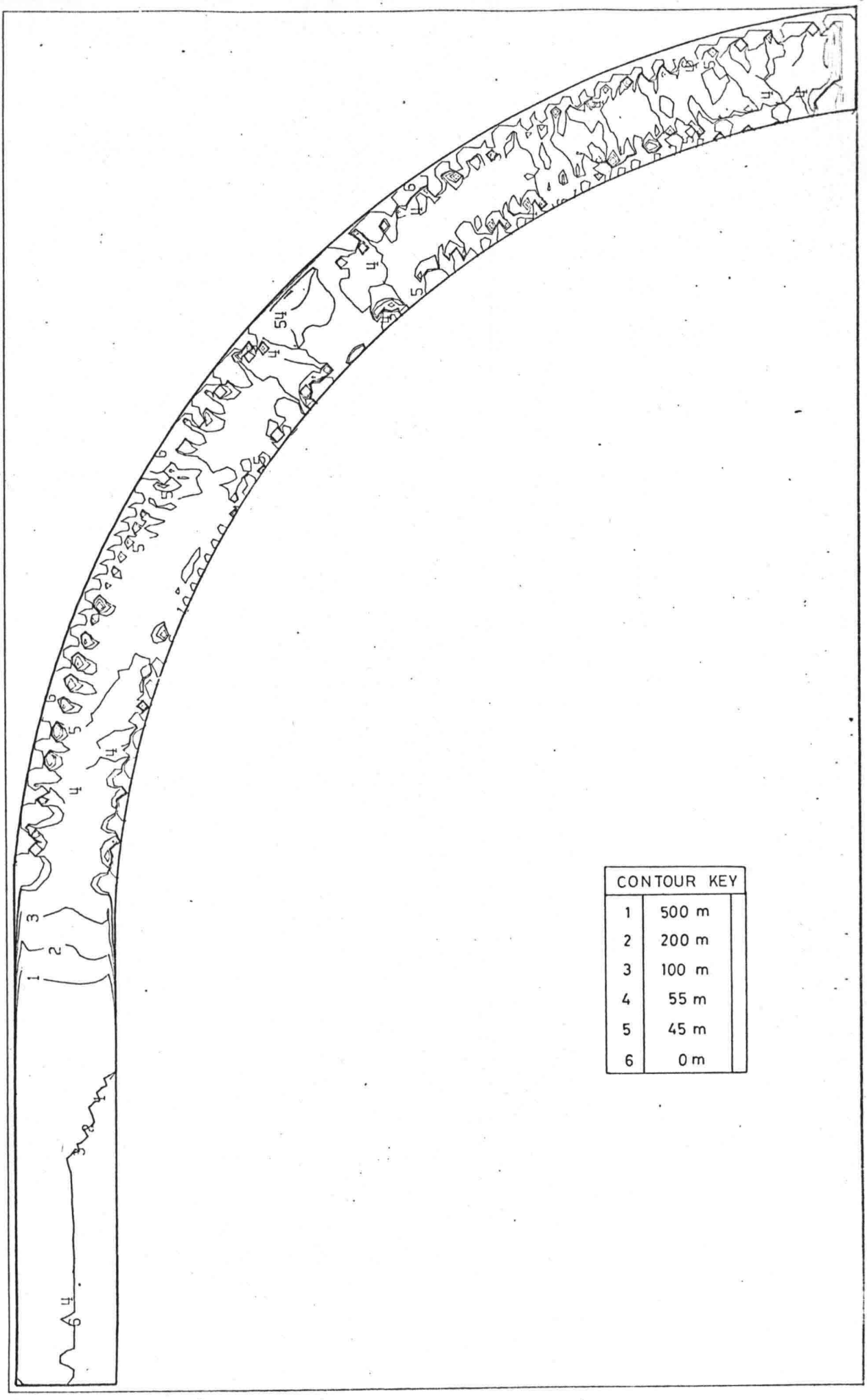

Fig. 24. Radius of curvature contour plot (uneven bed configuration)

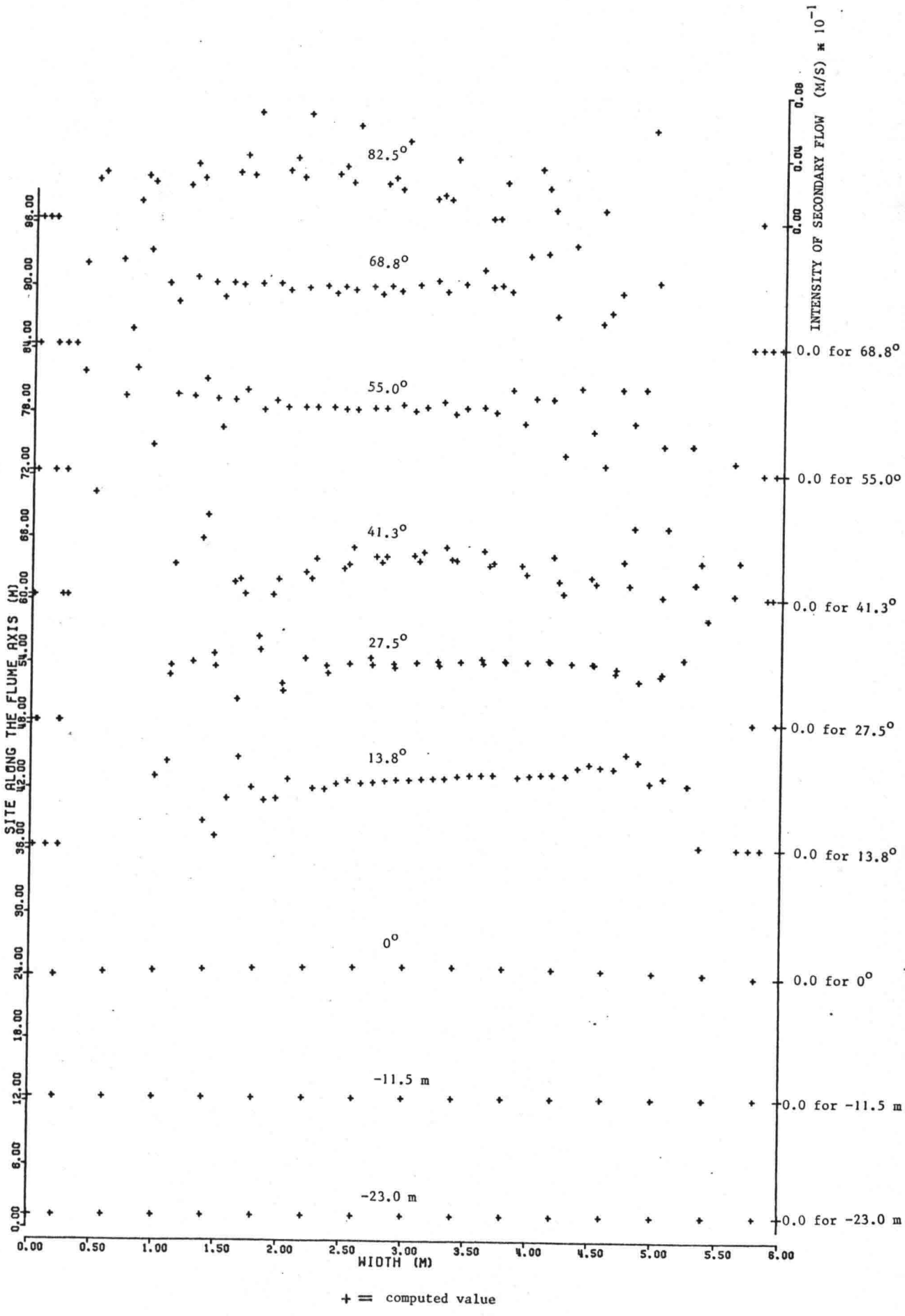

Fig. 25. Secondary flow intensity distributions in several cross-sections (plane bed configuration)

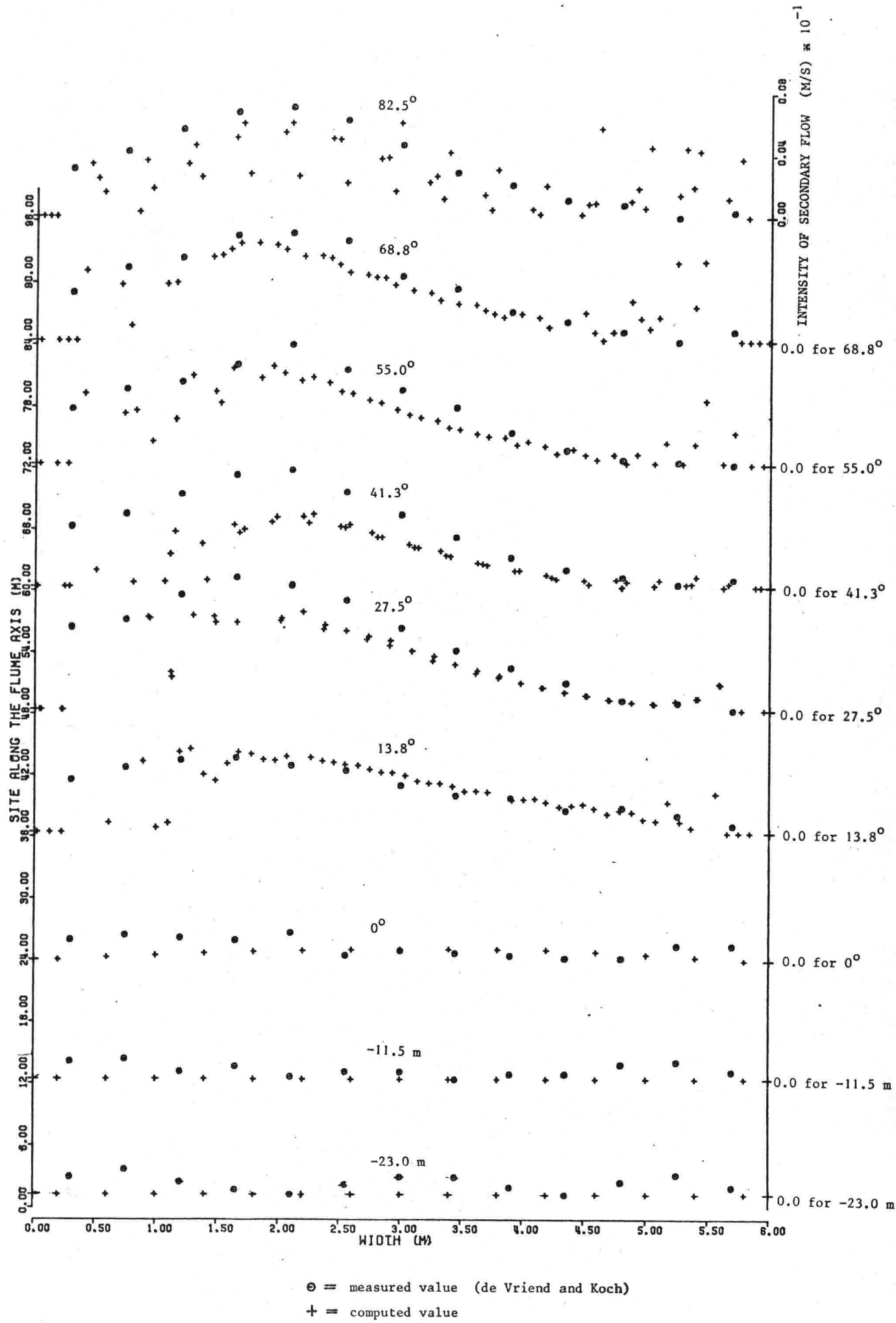

Fig. 26. Secondary flow intensity distributions in several cross-sections (uneven bed configuration)